An extended γ-tubulin ring functions as a stable platform in microtubule nucleation

Sarah Erlemann,[1] Annett Neuner,[1] Linda Gombos,[1] Romain Gibeaux,[2] Claude Antony,[2] and Elmar Schiebel[1]

[1]Zentrum für Molekulare Biologie der Universität Heidelberg, DKFZ–ZMBH Allianz, 69120 Heidelberg, Germany
[2]Cell Biology and Biophysics, European Molecular Biology Laboratory Heidelberg, 69117 Heidelberg, Germany

γ-Tubulin complexes are essential for microtubule (MT) nucleation. The γ-tubulin small complex (γ-TuSC) consists of two molecules of γ-tubulin and one molecule each of Spc97 and Spc98. In vitro, γ-TuSCs oligomerize into spirals of 13 γ-tubulin molecules per turn. However, the properties and numbers of γ-TuSCs at MT nucleation sites in vivo are unclear. In this paper, we show by fluorescence recovery after photobleaching analysis that γ-tubulin was stably integrated into MT nucleation sites and was further stabilized by tubulin binding. Importantly, tubulin showed a stronger interaction with the nucleation site than with the MT plus end, which probably provides the basis for MT nucleation. Quantitative analysis of γ-TuSCs on single MT minus ends argued for nucleation sites consisting of approximately seven γ-TuSCs with approximately three additional γ-tubulin molecules. Nucleation and anchoring of MTs required the same number of γ-tubulin molecules. We suggest that a spiral of seven γ-TuSCs with a slight surplus of γ-tubulin nucleates MTs in vivo.

Introduction

Microtubules (MTs) are dynamic polymers with functions in cell movement, intracellular transport, cell organization, and chromosome segregation. In cells, MT assembly is initiated at MT organizing centers, such as the mammalian centrosome or the yeast spindle pole body (SPB), by γ-tubulin, a member of the tubulin superfamily (Pereira and Schiebel, 1997). γ-Tubulin forms complexes with other proteins. The *Saccharomyces cerevisiae* γ-tubulin small complex (γ-TuSC) is a Y-shaped heterotetrameric complex consisting of two molecules of γ-tubulin (named Tub4 in yeast) and one molecule each of Spc97 (hSpc97 or GCP2 in mammals) and Spc98 (hSpc98 or GCP3; Marschall et al., 1996; Spang et al., 1996; Knop and Schiebel, 1997; Wiese and Zheng, 2006; Kollman et al., 2010).

In most eukaryotes, several γ-TuSC molecules assemble together with GCP4, GCP5, and GCP6 (GCP4–6) into the much larger γ-tubulin ring complex (γ-TuRC; Zheng et al., 1995). EM analysis of the purified γ-TuRC from *Drosophila melanogaster* identified a ringlike structure comprising repeated γ-TuSC subunits (Moritz et al., 2000). The position and function of GCP4–6 in the γ-TuRC remain a matter of debate (Moritz et al., 2000; Guillet et al., 2011). However, sequence alignment of GCP4–6 proteins with Spc97/GCP2 and Spc98/GCP3 identified two conserved regions between these proteins that have been named the GRIP1 and GRIP2 motifs. It was recently established that GCP4 probably binds to γ-tubulin via the GRIP2 domain, suggesting a direct role for GCP4 in γ-tubulin organization within the γ-TuRC (Guillet et al., 2011).

S. cerevisiae does not encode orthologs of γ-TuRC proteins, MT severing proteins, or additional MT minus-end binding proteins such as *Drosophila* patronin (Goodwin and Vale, 2010; Hutchins et al., 2010; Kollman et al., 2011). Furthermore, MT nucleation in budding yeast is only promoted by γ-TuSC that is bound to the nuclear and cytoplasmic sides of the SPB by the receptor proteins Spc110 and Spc72, respectively (Knop and Schiebel, 1997, 1998; Nguyen et al., 1998). After nucleation, MTs remain anchored to the SPB through the docking of the capped MT minus ends to Spc110 and Spc72 (Byers et al., 1978; Pereira et al., 1999). Moreover, the SPB organizes a defined number of nuclear MT (nMTs) and cytoplasmic MTs (cMTs). EM revealed that there are only 21–25 MTs in haploid yeast cells (O'Toole et al., 1999; Giddings et al., 2001;

Correspondence to Elmar Schiebel: e.schiebel@zmbh.uni-heidelberg.de

Abbreviations used in this paper: cMT, cytoplasmic MT; FLIP, fluorescence loss in photobleaching; γ-TuRC, γ-tubulin ring complex; γ-TuSC, γ-tubulin small complex; KT, kinetochore; MT, microtubule; nMT, nuclear MT; PSF, point spread function; ROI, region of interest; SC, synthetic complete; sfGFP, superfolder GFP; SPB, spindle pole body.

The Rockefeller University Press $30.00
J. Cell Biol. Vol. 197 No. 1 59–74
www.jcb.org/cgi/doi/10.1083/jcb.201111123

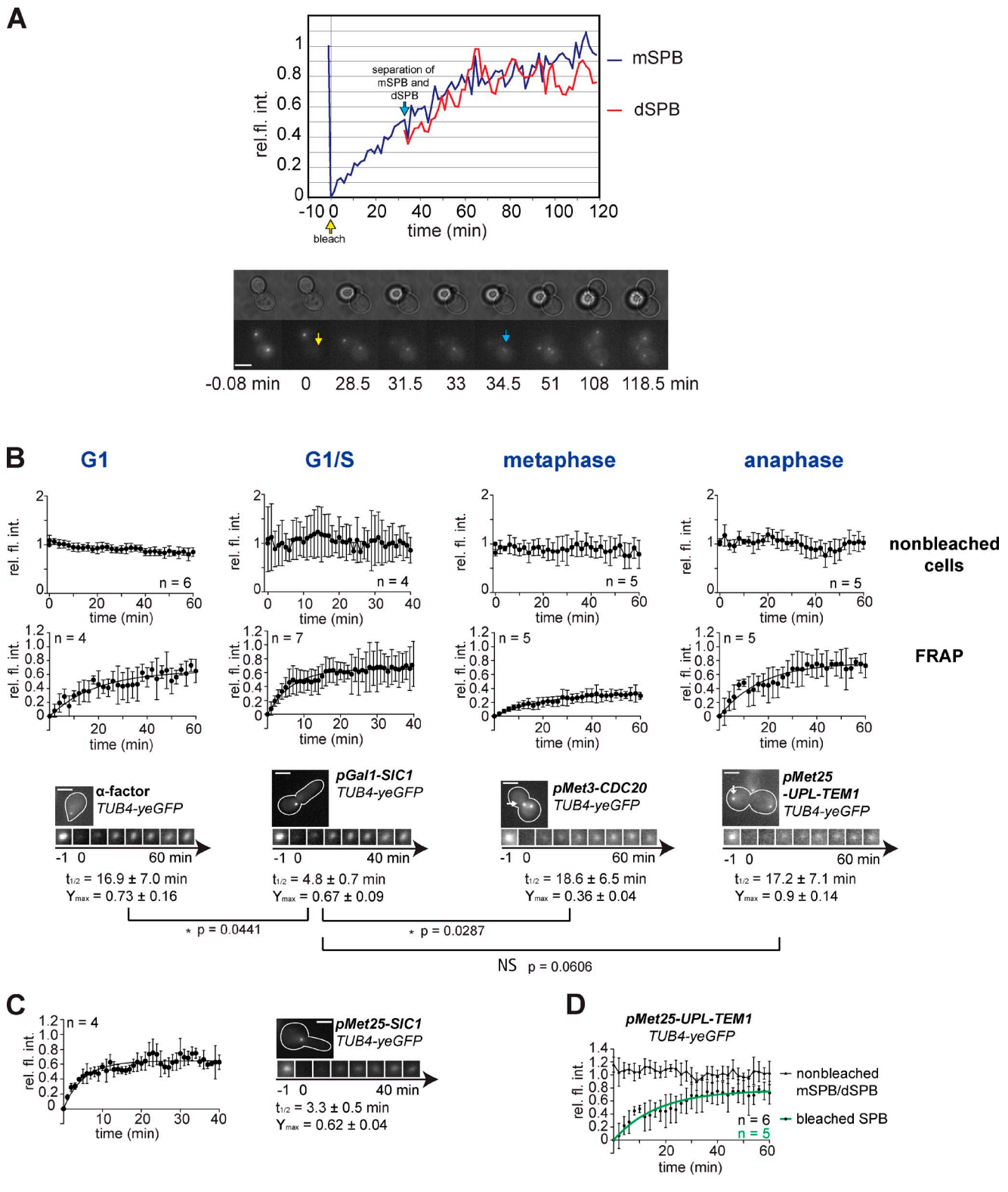

Figure 1. **Dynamic properties of Tub4 at SPBs.** (A) Photobleaching of Tub4-yeGFP at the SPB in a nonsynchronized cell. The SPB of the cell shown on the bottom was bleached in late anaphase (yellow arrow) and then was monitored for 2 h over the next cell cycle. After separation of mother SPB (mSPB) and daughter SPB (dSPB; blue arrow), the relative fluorescence intensities (rel. fl. int.) of both the mother and daughter SPBs were measured over time. (B) Tub4-yeGFP FRAP experiments of cells arrested in G1 with α-factor, G1/S by *SIC1* overexpression, metaphase by Cdc20 depletion, and anaphase by Tem1 depletion. The Tub4-yeGFP signal at SPBs was bleached with a laser pulse (time −1), and the recovery was followed over time. The mean relative fluorescence signal of nonbleached cells with SD error bars (top), the fitted mean FRAP recovery curves with SD error bars (middle), and examples of bleached cells (bottom) are shown. The mean of $t_{1/2}$, Y_{max} ± SEM, and p-values from the *t* test for Y_{max} by comparison with *SIC1* overexpression are given at the bottom. Arrows indicate the recovery of Tub4-yeGFP signal over time. (C) As in B (*pGal1-SIC1*) but with *pMet25-SIC1* cells to show that the growth conditions do not influence the outcome of the experiment. (D) *TUB4-yeGFP pMet25-UPL-TEM1* cells were arrested in anaphase by Tem1 depletion. One of the SPBs was bleached with a laser pulse, and the relative fluorescence intensities of both SPBs in the cells were followed over time. Fitted mean FRAP

Khmelinskii et al., 2009). Thus, *S. cerevisiae* has a basic and very well-defined MT system.

The favored model for MT nucleation is the template model (Pereira and Schiebel, 1997; Kollman et al., 2011), in which γ-tubulin assembles into a ring of 13 molecules that form a template for the nucleation of MTs with 13 tubulin protofilaments (Kilmartin, 1981; Pereira and Schiebel, 1997; Pereira et al., 1999; Kollman et al., 2010, 2011). This model is supported by the finding that in vitro, the purified yeast γ-TuSC assembles into spirallike filaments of 13 γ-tubulin molecules per turn (Kollman et al., 2010). However, it is unclear how many γ-tubulin molecules are required for MT nucleation and anchorage in vivo. Here, we have addressed this question by quantifying numbers of γ-TuSCs at SPBs and single detached cMTs. Approximately seven γ-TuSCs with a slight surplus of γ-tubulin molecules nucleate and anchor MTs at SPBs in cells. In addition, we provide evidence that oligomers of γ-TuSC form a stable high-affinity platform for the recruitment of α/β-tubulin heterodimers.

Results

The yeast γ-TuSC is stably bound to the SPB throughout the cell cycle

Very little is known about the structure and properties of MT nucleation sites in budding yeast cells apart from the fact that overexpression data indicate that only the SPB-associated γ-TuSC is able to nucleate MTs in the cell (Pereira et al., 1998). To understand the properties of the γ-TuSC at SPBs in cells, we used FRAP to ask whether γ-tubulin is stably bound to SPBs. FRAP experiments were performed with cells carrying *TUB4-yeGFP* (*TUB4* fused to yeast codon-adapted enhanced GFP) at its endogenous locus. The functionality of *TUB4-yeGFP* and other yeGFP-tagged γ-TuSC constructs was verified by growth assays and genetic interaction tests (Fig. S1).

Initial FRAP experiments with cycling cells showed that the Tub4-yeGFP signal recovered very slowly over ∼100 min (Fig. 1 A). This indicates that Tub4-yeGFP is stably bound to SPBs. To determine whether the dynamics of Tub4-yeGFP at SPBs is cell cycle regulated, we performed FRAP experiments with cells in which cell cycle progression had been arrested at defined cell cycle phases. The Tub4-yeGFP signal at SPBs of unbleached arrested cells remained constant throughout the experiment irrespective of the cell cycle state, indicating that the observed recovery reflected subunit exchange rather than growth of the SPB (Fig. 1 B, nonbleached cells). The half recovery time ($t_{1/2}$) for cells in G1 (α-factor), metaphase (*CDC20* depletion), and anaphase (*TEM1* depletion) ranged between 17 and 19 min (Fig. 1 B). In contrast, Tub4-yeGFP of cells in G1/S phase (G1/S arrest was induced by *SIC1* overexpression from the pGal1 or pMet25 promoter; Fig. 1, B and C) exchanged with a $t_{1/2}$ of 3.3–4.8 min, which is significantly faster than for cells in G1, metaphase, or anaphase. The maximal recovery (Y_{max}) was between 62 and 90% for cells in G1, G1/S, and anaphase (Fig. 1 B). However, in metaphase cells, Y_{max} was reduced to 36%, which indicates a large immobile Tub4 pool of 64% at SPBs. We conclude that the Tub4 exchange at SPBs is slow, with a peak in mobility in G1/S.

In Fig. 1 B, the recovery of the SPB signal could be impaired because we bleached most of the cellular Tub4-yeGFP pool. In such a case, we would not see fast recovery even when Tub4-yeGFP is highly dynamic. However, we found that the Tub4-yeGFP signal at the second nonbleached SPB of anaphase cells was not affected by bleaching only one of the two SPBs (Fig. 1 D). This result further indicates slow exchange of Tub4 at SPBs.

The residence time of α/β-tubulin at γ-tubulin nucleation sites is higher than that at MT plus ends

The MT depolymerizing drug nocodazole binds to the same site on β-tubulin as colchicine. This binding changes tubulin from the straight to a curved conformation. The conformational switch blocks the interaction between tubulin subunits and therefore induces MT depolymerization (Ravelli et al., 2004; Nguyen et al., 2005). However, in yeast γ-tubulin, the amino acid residues that mediate binding to colchicine are not conserved (Fig. 2 A, amino acids in red). Therefore, Tub4 lacks the high-affinity colchicine/nocodazole-binding site of β-tubulin. Thus, as γ-tubulin interacts with the α-tubulin subunit of tubulin, it is unlikely that nocodazole blocks interaction of tubulin with γ-tubulin, even though it impairs binding between α/β-tubulin heterodimers. Consistent with this notion, nocodazole treatment depolymerized all MTs, with the exception of tubulin remnants that remained bound to kinetochores (KTs; Fig. 2 B, arrows) and SPBs (Fig. 2 B, arrowheads). SPB binding of α/β-tubulin heterodimers in nocodazole-treated cells was reliant on γ-tubulin (the SPB marker Spc42 lacks a Tub2 signal; Fig. 2 B, *tub4Δ*). In contrast, binding of Tub2 to KTs was independent of γ-tubulin function (Fig. 2 B, *tub4Δ* [Tub2 signal marked with an arrow]; Kitamura et al., 2010). This suggests that the tubulin signal at SPBs represents nocodazole-resistant interactions between SPB-associated MT nucleation sites and tubulin subunits.

The MT remnants at SPBs in nocodazole-arrested cells provided the opportunity to analyze the interaction between α/β-tubulin heterodimers and γ-tubulin at SPBs in vivo. GFP-Tub1 remnants at SPBs of nocodazole-treated cells rapidly exchanged with a $t_{1/2}$ of 7.4 s (k_{off} = 0.094 s^{-1}) and a maximal recovery Y_{max} of 69% (Fig. 2 C). Fluorescence loss in photobleaching (FLIP) of GFP-Tub1 further verified a rapid exchange of >90% of GFP-Tub1 at SPBs (Fig. 2 D). Thus, nearly all of the GFP-Tub1 at SPBs of cells incubated in nocodazole is mobile.

recovery curves with SD error bars of bleached SPBs are shown in green; the mean of nonbleached SPBs of cells used for FRAP experiments with SD error bars are shown in black. *n*, number of analyzed SPBs. Bars: (A–C) 4 µm; (B and C, magnified SPB images) 1.41 $µm^2$.

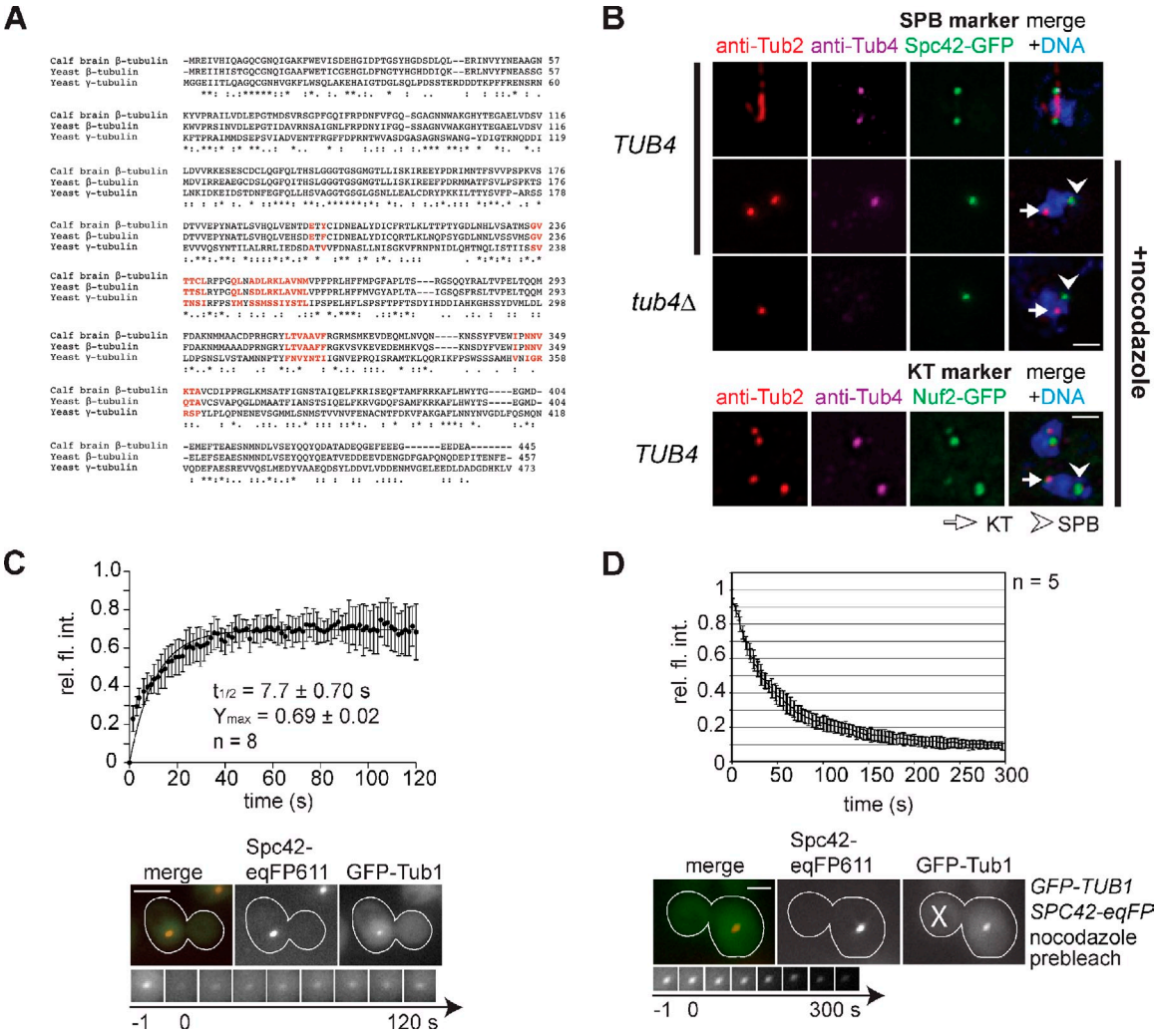

Figure 2. **Analysis of αβ-tubulin–γ-tubulin interactions.** (A) Comparison of colchicine-binding site in β-tubulin with the sequence in yeast γ-tubulin. An alignment of calf brain β-tubulin with *S. cerevisiae* β-tubulin (*TUB2*) and γ-tubulin (*TUB4*) is shown. The sequence alignment was created with CLUSTALW 2.0.12 (Chenna et al., 2003). Asterisks indicate identical residues. Conserved residues are indicated by two dots and semiconserved residues by one dot. Residues, which interact with colchicine, are marked in red. (B) Analysis of binding of tubulin to KTs and SPBs. *SPC42-yeGFP* and *NUF2-yeGFP* cells were incubated with or without nocodazole. Cells were fixed and prepared for indirect immunofluorescence. *TUB4* auxin degron cells (*tub4Δ*; Nishimura et al., 2009) with *SPC42-yeGFP* were analyzed after auxin addition and Tub4 depletion by indirect immunofluorescence with anti-Tub2 and anti-Tub4 antibodies. DNA was stained with DAPI. Bars, 5 µm. (C) *GFP-TUB1 SPC42-eqFP611* cells were incubated with nocodazole for 1 h after synchronization with α-factor. GFP-Tub1 at the SPB was bleached with a laser pulse, and the recovery was followed over time. The fitted mean FRAP recovery curves with SD error bars are shown (top). An example of a bleached cell over time is shown (bottom). *n*, number of analyzed cells; rel. fl. int., relative fluorescence intensity. (D) FLIP experiment of *GFP-TUB1 SPC42-eqFP* cells. The cells were synchronized with α-factor and subsequently released into YPAD medium with nocodazole until cells had arrested with a large bud in metaphase. The daughter cells were consecutively bleached, and the intensities of GFP-Tub1 at SPBs were recorded. (top) Mean graphs of relative intensities at the SPB with SD error bars. (bottom) Image of a representative bleached cell over time. X indicates the bleached region in the daughter cell. Bars: (C) 4 µm; (C, magnified SPB images) 2.44 µm^2; (D) 2 µm; (D, magnified SPB images) 2.06 µm^2.

To test whether the tubulin remnants in nocodazole-treated cells stabilize the γ-TuSC at the SPB, we conducted FRAP analysis of Tub4-yeGFP at SPBs in wild-type and *tub2-403* cells (mutation in the yeast β-tubulin gene). Before the experiment, both strains were incubated with nocodazole to arrest the cells in metaphase. Importantly, in the presence of nocodazole, *tub2-403* cells did not show a tubulin signal (anti-Tub2) at SPBs and at KTs, whereas a Tub4-yeGFP signal persisted at SPBs (Fig. 3 A). Thus, comparing the Tub4-yeGFP signal at wild-type and *tub2-403* SPBs in the presence of nocodazole will indicate whether the α-tubulin–Tub4 interaction stabilizes the population of Tub4 that resides at SPBs. During the course of the experiment, Tub4-yeGFP of unbleached cells remained constant (Fig. 3 B, top). In the FRAP experiment, the $t_{1/2}$ of Tub4-yeGFP was significantly reduced from 11.3 (*TUB2*) to 7.2 min (*tub2-403*), suggesting that the α-tubulin–γ-tubulin interaction helps to further stabilize γ-TuSCs at SPBs (Fig. 3 B, bottom). Noteworthy, the Y_{max} of 28–29% in the FRAP experiment with nocodazole cells (Fig. 3 B) was similar to that of cells arrested in metaphase as a consequence of Cdc20 depletion (36%; Fig. 1 B). Collectively, these data establish that γ-TuSCs exist as a relatively stable MT nucleation platform at SPBs. This platform recruits tubulin subunits that contribute to further stabilization SPB-associated γ-TuSCs.

Stoichiometry and number of γ-TuSCs and its receptors at MT nucleation sites

Next, we addressed how many γ-TuSC molecules are required to organize MTs in vivo. The intensity of a GFP signal is directly proportional to the number of the GFP-tagged proteins at any given location (Wu and Pollard, 2005). To determine the number of γ-TuSC molecules at the SPBs of metaphase and anaphase cells, the yeGFP signal of SPB-associated γ-TuSC components was compared with that of budding yeast CENP-A homolog Cse4-yeGFP (Fig. S2 A). As the copy number of Cse4 is the same for every KT, it is widely used as a standard reference value for quantification of GFP signals (Jin et al., 2000; Joglekar et al., 2006; Coffman et al., 2011; Lawrimore et al., 2011). We also used rotavirus-like particles (EGFP-VP2/VP6) that contain 120 EGFP molecules per virus as an additional reference (Fig. S2 A; Charpilienne et al., 2001; Dundr et al., 2002).

We first confirmed the linearity between exposure time and fluorescence signal intensity of our microscope (Fig. S2 B). In addition, light intensity fluctuations of the microscope light source did not influence the outcome of the measurements (Fig. S2 C). Furthermore, we confirmed the ratio of signal intensities of Cse4-yeGFP and Nuf2-yeGFP at clustered KTs of metaphase and anaphase cells (Fig. S2 D [i]; Joglekar et al., 2006). The KT signal from *NUF2-yeGFP CSE4-yeGFP* cells was approximately the sum of the GFP signals from two cells, one expressing *NUF2-yeGFP* and the other expressing *CSE4-yeGFP* (Fig. S2 D [i]). The signal of *CSE4-yeGFP/CSE4-yeGFP* diploid cells was twice of that of haploid *CSE4-yeGFP* cells (Fig. S2 D [i]). Likewise, the SPB signal of *SPC72-yeGFP SPC110-yeGFP* cells was approximately the sum of the signal of *SPC72-yeGFP* and *SPC110-yeGFP* cells (Fig. S2 D [iii]). The fluorescence signal of diploid *TUB4-yeGFP/TUB4-yeGFP* cells was approximately twice as high as the signal of haploid cells (Fig. S2 D [iii]). Similar signals for yeGFP-Spc97 and Spc97-yeGFP were measured per SPB, indicating that the position of the tag did not influence the outcome (Fig. S2 D [ii]). A comparison between Tub4-yeGFP and the fast-folding Tub4-sfGFP (superfolder GFP; Pédelacq et al., 2006) gave similar results when compared with the corresponding Cse4-yeGFP or Cse4-sfGFP reference (Fig. S2 D [ii]), suggesting that the yeGFP tag at Tub4 is properly folded at SPBs. Together, these controls show that the GFP measurements were accurate, sensitive, and performed within a linear range.

Next, the GFP signals of Tub4-yeGFP, Spc97-yeGFP, Spc98-yeGFP, Spc110-yeGFP, and Spc72-yeGFP were measured at metaphase and anaphase SPBs (Fig. 4 A). For each measurement, the γ-TuSC–yeGFP signal was calibrated by the Cse4-yeGFP signal of cells that were present on the same coverslip. The signal distribution of γ-TuSC proteins and the receptor proteins Spc110 and Spc72 showed a Gaussian distribution, indicating that a similar number of each of these proteins was associated with SPBs (Fig. 4 B). The metaphase and anaphase signals for Tub4-yeGFP, Spc97-yeGFP, and yeGFP-Spc98 at SPBs were very similar (Figs. 4 C and S2 D [iii]). The molar ratio of Tub4/Spc97/Spc98 at SPBs was ~2.7:1.1:1. The fact that the ratio between Tub4 and Spc97/Spc98 was greater than twofold suggests that either Tub4 binds to SPBs independently of γ-TuSCs or that Tub4 monomers oligomerize with γ-TuSCs to generate larger complexes.

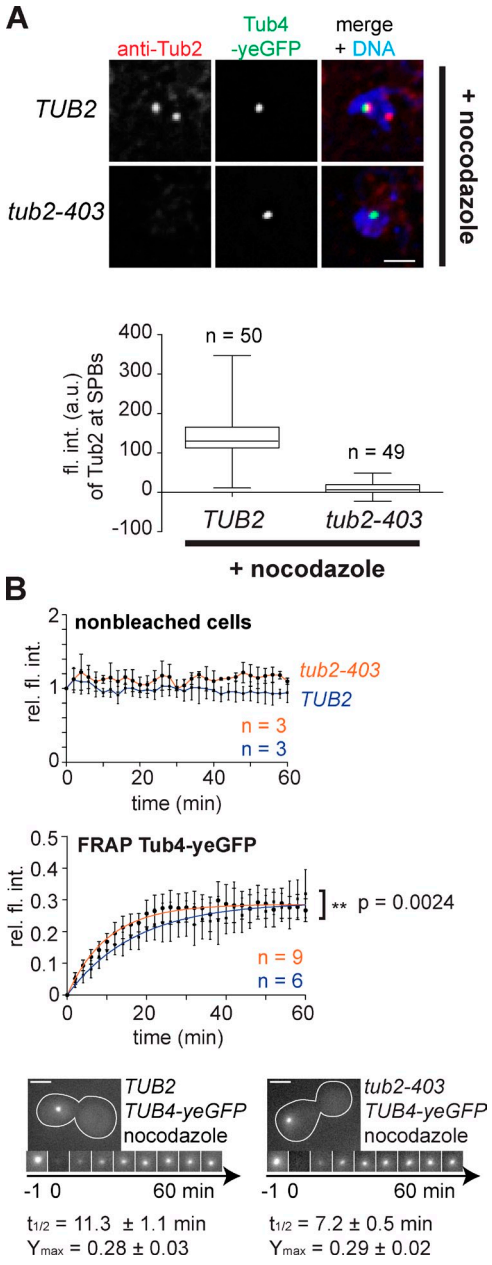

Figure 3. **Influence of αβ-tubulin on γ-tubulin binding to the SPB.** (A) Localization of β-tubulin at SPBs in *TUB2* wild-type and *tub2-403* cells with *TUB4-yeGFP*. Both cell types were synchronized with α-factor, subsequently incubated with nocodazole, fixed, and stained with anti-Tub2 antibodies. (top) Images of fixed cells. Signals of anti-Tub2, Tub4-GFP, and stained DNA (blue) are shown. (bottom) Quantification of absolute intensities of anti-Tub2 at the SPB in *tub2-403* and *TUB2* cells. *n*, number of analyzed SPBs; fl. int., fluorescence intensity; a.u., arbitrary unit. (B) FRAP experiments of Tub4-yeGFP of *TUB2* and *tub2-403* cells treated with nocodazole for 1 h after synchronization with α-factor. (top) Relative fluorescence intensity (rel. fl. int.) of nonbleached cells. (middle) Mean FRAP recovery curve with SD error bars. (bottom) Images of photobleached cells and mean of $t_{1/2}$ and Y_{max} ± SEM are shown. The *t* test (**, P = 0.0024) is for the $t_{1/2}$ of the experiment. Bars: (A and B) 5 µm; (B, magnified SPB images) 2.7 µm^2.

In budding yeast, most MTs (85–90%) are organized by γ-TuSCs bound to the SPB via the nuclear receptor Spc110 (Knop and Schiebel, 1998; Nguyen et al., 1998). This suggests that the majority of γ-TuSCs are at the nuclear side of the SPB.

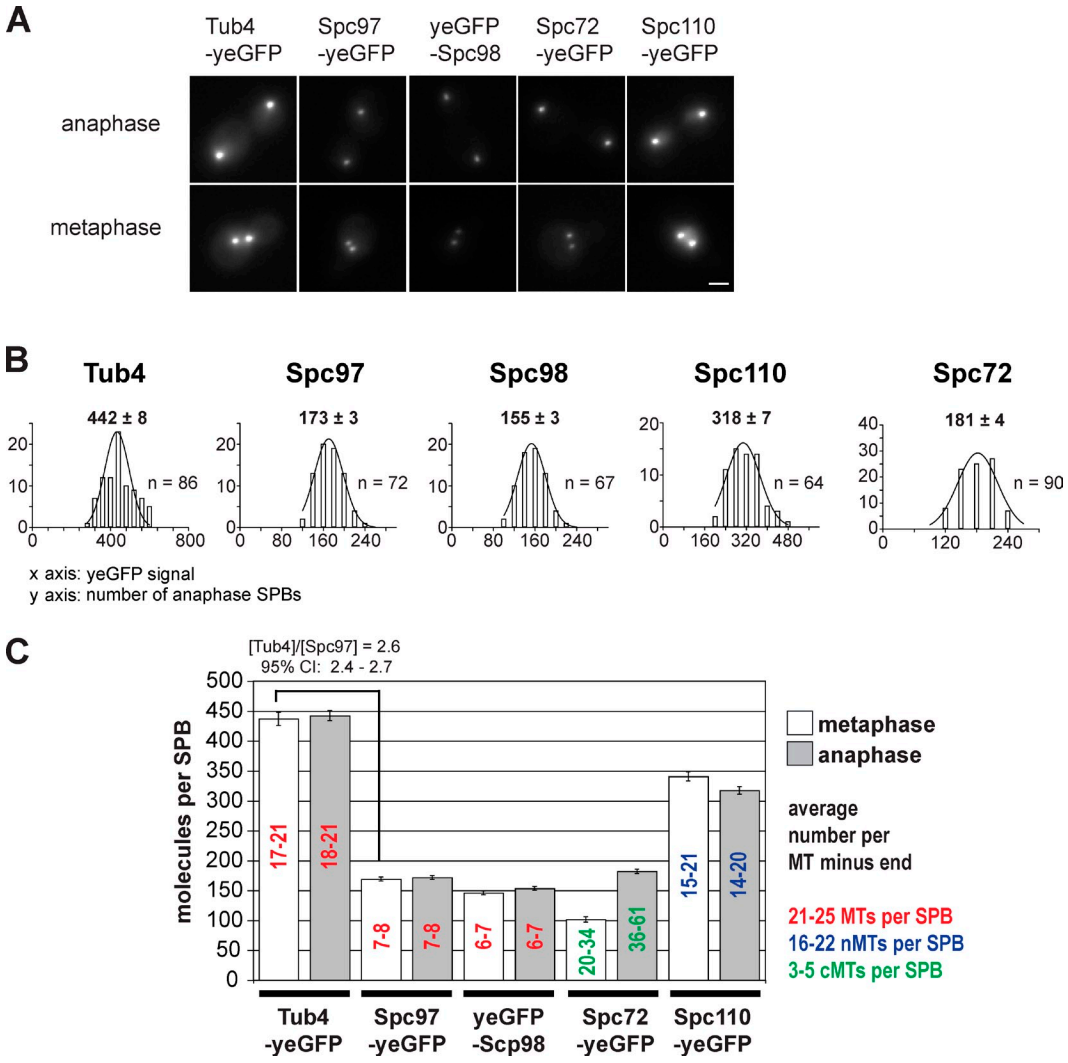

Figure 4. **Quantification of γ-TuSC proteins and receptors at SPBs.** (A) Tub4-yeGFP, Spc97-yeGFP, yeGFP-Spc98, Spc72-yeGFP, and Spc110-yeGFP signal at SPBs of metaphase and anaphase cells. Bar, 2 µm. (B) γ-TuSC signal at the SPB in anaphase cells. Mean signals ± SEM are given. *n*, number of analyzed SPBs. (C) Bar diagram of γ-TuSC, Spc72, and Spc110 numbers at the SPB in meta- and anaphase cells with SEM error bars. The molecule numbers were calculated by comparison of the corresponding yeGFP signals to Cse4-yeGFP as a reference. Numbers of yeGFP-tagged proteins per single MT minus end are also given in the diagram (red, cMT and nMT; green, cMT; and blue, nMT). [Tub4]/[Spc97] is the ratio of Tub4 to Spc97. CI, confidence interval.

In this context, the Spc97-Spc98/Spc110 fluorescence ratio was close to 1:2. This ratio is consistent with the finding that the N terminus of Spc110 interacts with both Spc97 and Spc98 (Geissler et al., 1996; Knop and Schiebel, 1998; Nguyen et al., 1998).

Next, we measured the absolute number of γ-TuSC, Spc110, and Spc72 molecules at each SPB. Recently, the number of Cse4 molecules per yeast KT was determined to be 5.2 (mean for two endogenously tagged strains; Lawrimore et al., 2011). We confirmed the number of approximately five Cse4-EGFP molecules per KT using reconstituted rotavirus capsids (EGFP-VP2/VP6; Fig. S2 E; Charpilienne et al., 2001; Dundr et al., 2002). Thus, the cluster of 16 KTs of a haploid yeast cell consists of 83 Cse4-yeGFP molecules.

Taking 83 Cse4 molecules per haploid KT cluster into account, the number of Tub4, Spc97, Spc98, Spc110, and Spc72 molecules per haploid SPB was determined to be 442, 173, 155, 318, and 181, respectively, for anaphase cells (Fig. 4 C). The numbers of molecules in metaphase cells were similar except for Spc110 and Spc72. The Spc110 metaphase number was slightly higher (P = 0.0482), whereas Spc72 in metaphase was half of the anaphase number. In several independent measurements, we confirmed these numbers for Tub4, Spc72, and Spc110 at haploid SPBs either using EGFP-VP2/VP6 particles or *NUF2-yeGFP* cells as the internal standard (Fig. S2, E [i] and F). Moreover, the number of molecules did not vary between independently constructed yeast strains (Fig. S2 D [iii]; the numbers for Tub4 and Spc110 are shown).

By dividing the numbers of γ-TuSC molecules by the number of MTs per SPB (Winey et al., 1995; O'Toole et al., 1999; Khmelinskii et al., 2009), we obtained a mean of 17–21 Tub4, 7–8 Spc97, and 6–7 Spc98 molecules per MT in mitotic cells (Fig. 4 C, numbers in bars). Spc72 is specifically bound to the cytoplasmic side of the SPB, where it organizes three to five cMTs (Knop and Schiebel, 1998). The Spc72/cMT ratio was 20/cMT to 34/cMT for metaphase and 36/cMT to

61/cMT for anaphase cells. These values considerably exceed the numbers calculated for the Spc110/nMT ratio of 15/nMT to 21/nMT (metaphase) and 14/nMT to 20/nMT (anaphase) using 16–22 nMTs as a reference (Fig. 4 C). Thus, it is possible that a fraction of the Spc72 molecules that reside at SPBs does not anchor cMTs (Fig. 4 C) but may perform other functions (see Discussion).

Seven γ-TuSCs with three additional γ-tubulin molecules form a single MT nucleation site

For the calculation of the number of γ-TuSCs per MT, we assumed that all γ-TuSC molecules at SPBs are involved in MT nucleation and that all nucleation sites are identical. To measure the number of γ-TuSCs at MT minus ends directly and more accurately, we determined the yeGFP signal of tagged γ-TuSC proteins and the receptor Spc72 on single detached cMTs.

In G1 and in cells treated with mating pheromone, the SPB component Kar1 anchors Spc72 and cMTs to the cytoplasmic side of the SPB (Pereira et al., 1999). The Spc72 binding site of Kar1 is compromised in *kar1-Δ15* cells, leading to the detachment of cMTs upon incubation of cells with the mating pheromone α-factor (Pereira et al., 1999). These detached cMTs showed signals of Tub4-yeGFP, Spc97-yeGFP, yeGFP-Spc98, and Spc72-yeGFP at the minus ends (Fig. 5 A). Intensity profiles of the yeGFP and mCherry-Tub1 signals showed that γ-TuSC subunits and Spc72 abutted the cMT ends (Fig. 5 B). Proper alignment of the microscope optics was confirmed by measurement of fluorescent beads (Fig. S2 G). Importantly, the detached Spc72–γ-TuSC in the cytoplasm was competent to nucleate MTs, as shown by nocodazole washout experiments (Fig. 5 C; for additional examples, see Fig. S3 A). Renucleation of MTs by γ-TuSC attached to the nuclear side of the SPB resulted in a clearly stronger mCherry-Tub1 signal than at the detached Spc72–γ-TuSC complex (Fig. 5 C, asterisks vs. arrow). This clearly discriminates the detached cMT nucleation site from the SPB. Fig. S3 B shows examples of *SPC72-yeGFP* cells with additional *SPC42-yeGFP* or *SPC110-yeGFP*. The strong Spc42-yeGFP or Spc110-yeGFP signals unambiguously mark the SPB, whereas the weaker Spc72-yeGFP signal corresponds to the released nucleation site. Also in these cells, the detached nucleation sites formed MTs after nocodazole washout (Fig. S3 B).

Reconstitution of cMTs of α-factor–arrested *kar1-Δ15* cells by electron tomography revealed two to three single detached MTs in the cytoplasm in each cell (Figs. 6 [A and B] and S4). The minus ends of these detached cMTs were sealed by a closed cap (Fig. 6, red arrows in A1 and B1) in the same way as previously reported for the minus ends of nMTs at the inner face of the SPB (Fig. 6, A3 and B2; Byers et al., 1978). In contrast, the plus ends of cMTs (Fig. 6, A2) or nMTs (Fig. 6, A4 and B3 and B4) showed an open appearance. Additional examples of MT ends from *kar1-Δ15* cells are shown in Fig. S4. Together, these data establish that the detached cMTs in *kar1-Δ15* cells carry fully active MT nucleation sites.

Next, we counted γ-TuSC and Spc72 molecules on single detached cMTs. yeGFP signals of the four proteins showed a Gaussian distribution, indicating that most detached cMTs contain similar numbers of γ-TuSC and Spc72 molecules (Fig. 5 D). The ratio of Tub4/Spc97/Spc98/Spc72 signals was 2.4:1.0:1.3:2.1. Thus, MT nucleation sites contain a slight excess of Tub4 and Spc98 over what would be expected for γ-TuSC oligomers. In addition, two Spc72 molecules interact with one γ-TuSC on detached cMTs (Fig. 5 D).

The absolute number of γ-TuSC and Spc72 molecules on a single detached cMT was quantified using Cse4-yeGFP as a standard. 17 Tub4, 7 Spc97, 9 Spc98, and 15 Spc72 molecules were measured at each MT nucleation site. The difference between Spc97 and Spc98 was statistically significant, as was the greater than twofold excess of Tub4 over Spc97 (Fig. 5 D). Likewise, measuring Tub4-EGFP on single cMTs with viral particles as a reference also yielded the number of 17 Tub4 molecules per nucleation site (Fig. S2 E [ii]). A second *yeGFP-SPC98* clone confirmed that there was an excess of Spc98 over Spc97 at the ends of single cMTs (8.4 ± 0.4 Spc98 per MT for the second clone; $n = 65$, three independent datasets; $P = 0.394$ vs. the first clone). Collectively, these results suggest that the nucleation site consists of seven γ-TuSCs and an excess of approximately three Tub4 and approximately two Spc98 molecules. The nucleation site is anchored to SPBs via ∼15 Spc72 molecules, suggesting a ratio of one Spc72 dimer per γ-TuSC.

Identical numbers of Tub4 molecules are required for MT nucleation and anchorage at the SPB

In budding yeast, MT nucleation might be restricted to G1/S when SPBs duplicate (Marschall et al., 1996). In other phases of the cell cycle, MTs are anchored to the SPB through the physical interaction between Spc97 and Spc98 and the receptor proteins Spc72 and Spc110. As the requirements for MT nucleation and anchorage might differ, it is possible that nucleation in G1/S could rely upon a different number of γ-tubulin molecules than anchorage to SPBs in S phase or mitosis. However, quantifying signals at G1/S SPBs is challenging because the new SPB develops immediately adjacent to the preexiting old SPB. Thus, incorporation of proteins into the newly forming SPB in G1/S will consistently increase the signal for γ-TuSC, Spc110, and Spc72 simply because the new SPB is growing during the period of observation. This will obscure differences that arise from changes that are associated with a switch from MT nucleation to anchorage. In addition, in arrested G1/S cells, MTs are already formed at the new SPB. However, if different γ-TuSC numbers are involved in nucleation and anchorage, we would expect to see cell cycle–dependent changes in γ-TuSC numbers after SPB separation. Therefore, we measured the signal intensities of yeGFP fusion proteins of γ-TuSC components and its receptors by live-cell imaging. The γ-TuSC signals at SPBs rapidly doubled in G1/S phase during SPB duplication ($t = 0$; separation of side-by-side SPBs; note that the signal per SPB remained constant; Fig. 7 A). The yeGFP signal (Tub4-yeGFP, Spc97-yeGFP, and yeGFP-Spc98) dropped by 50% as soon as the mother and daughter SPBs split at the end of S phase and then remained relatively constant during mitosis (Fig. 7 A). The levels of Spc110-yeGFP at SPBs were

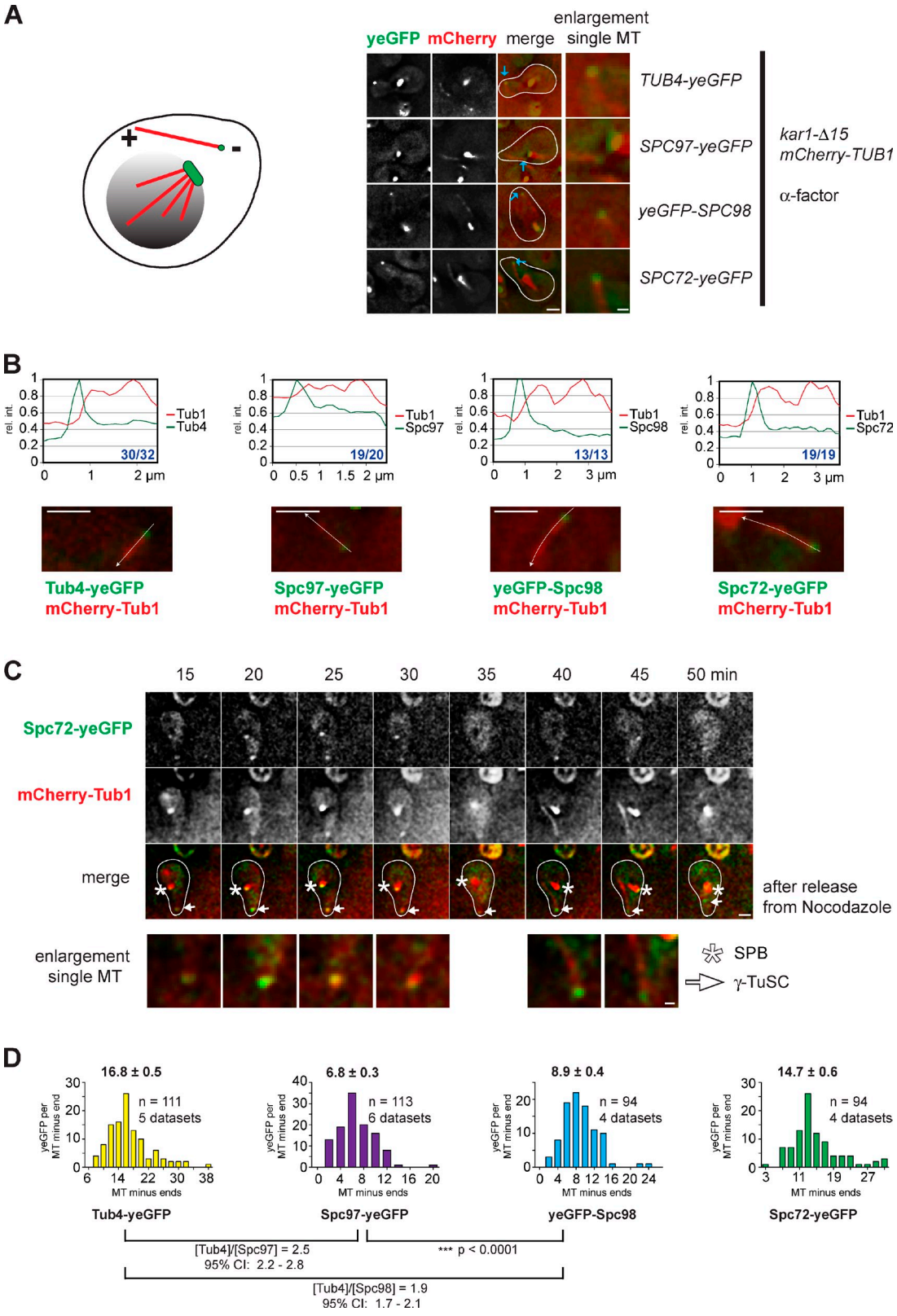

Figure 5. **γ-TuSC molecules at free cMT minus ends.** (A) *kar1-Δ15 mCherry-TUB1* cells with the indicated yeGFP-tagged genes were incubated with α-factor. This triggered detachment of cMTs from the SPB (illustrated in the cartoon). The images in the middle show cells with detached cMTs (single planes from z stacks). Pictures on the right show enlargements of detached cMTs. Blue arrows indicate minus ends of detached MTs. (B, top) Plot profiles of representative detached cMTs. Red lines indicate the signals of tagged cMTs, and green lines indicate the signals of tagged γ-TuSC proteins or Spc72 on MT minus ends. The numbers in the graph indicate MTs with yeGFP signals at MT ends versus the total number of analyzed MTs. rel. int., relative intensity. (bottom) Images of the cMTs that were used to create plot profiles (single planes from z stacks). The long white arrows indicate the region used for the line scans. (C) Functionality of detached γ-TuSC in MT nucleation. α-factor–arrested and nocodazole-treated *kar1-Δ15* cells were washed with medium

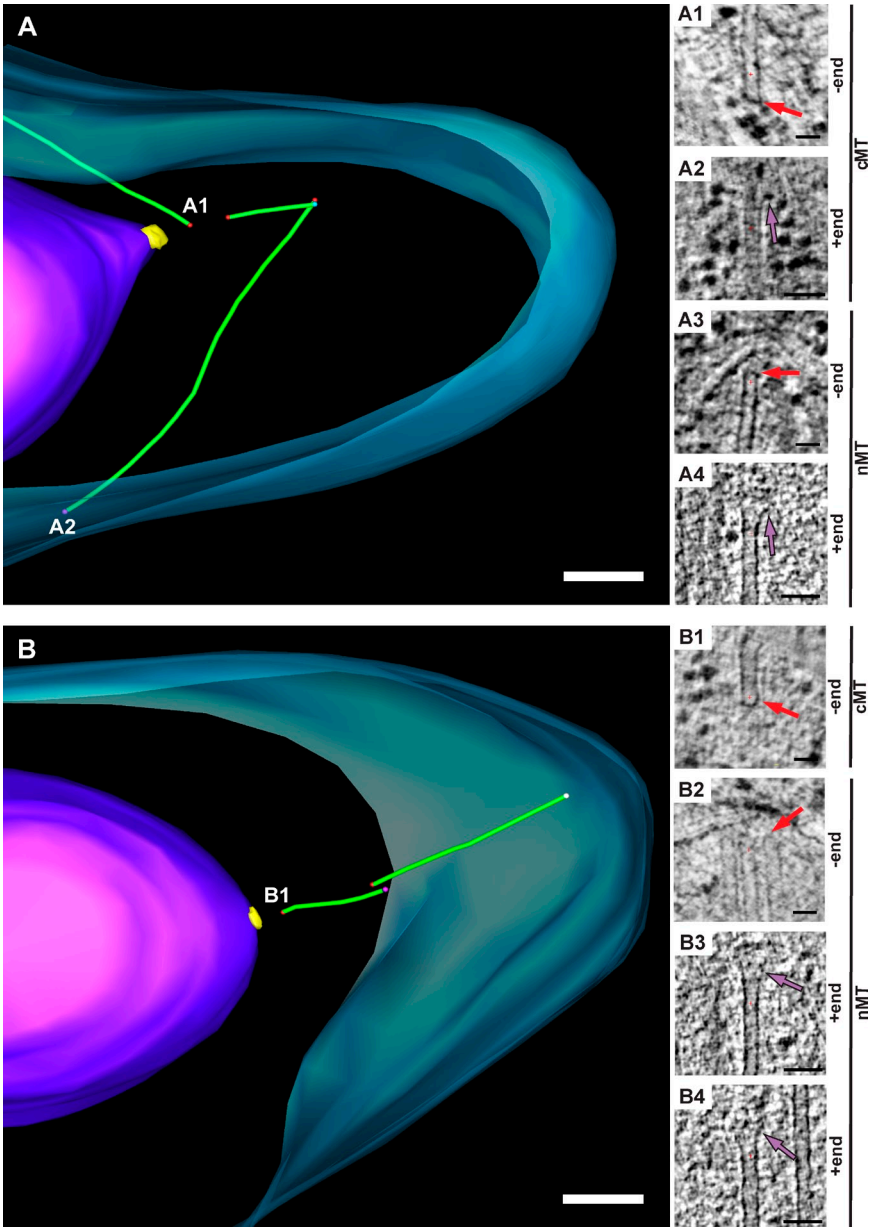

Figure 6. **Analysis of detached cMTs by electron tomography in *kar1-Δ15* cells.** (A) 3D model of an α-factor–treated *kar1-Δ15* cell with three single detached cMTs. Green lines indicate cMTs, purple indicates the nuclear envelope, and blue indicates the plasma membrane. Red dots indicate MT minus ends. Purple, white, and blue dots mark open MT plus ends with different conformations (flared, curled, and blunt). (A1–4) Electron tomograms of MTs and their end structures from the cell on the left. MTs were tracked using the slicer tool in the IMOD software package. (A1) Closed minus end of a single detached cMT (corresponds to the MT end labeled with A1 on the left. (A2) Open plus end of a single detached cMT (A2 on the left). (A3) Closed minus end of an nMT. (A4) Open plus end of an nMT. (A1 and A3) Red arrows denote closed MT minus ends. (A2 and A4) Purple arrows indicate open MT plus ends. (B) 3D model of another α-factor–treated *kar1-Δ15* cell with two single detached cMTs. Color coding is as in A. (B1) Electron tomogram of a closed minus end of a single detached cMT (B1 on the left). (B2) Closed minus end of an nMT. (B3 and B4) Open plus ends of two nMTs. (B1–4) Color coding of arrows is as in A1–4. Bars: (A and B) 300 nm; (A1, A3, B1, and B2) 30 nm; (A2, A4, B3, and B4) 50 nm.

slightly higher in metaphase versus anaphase (Fig. 7 B; see also Figs. 4 C and S2 D [iii]). The Spc72-yeGFP signal started to increase in mitosis to peak upon maximal extension of the anaphase spindle (see also Fig. 4 C).

Next, we asked whether the composition of the Tub4 complex differed between the phases of MT nucleation and stable MT attachment. MT reassembly in response to nocodazole washout reflects MT nucleation, as tubulin remnants at SPBs are only loosely bound in nocodazole-arrested cells (Fig. 2). We synchronized *TUB4-yeGFP* cells by α-factor in G1 phase before releasing them into medium with nocodazole. Cells progressed through S phase and finally arrested in mitosis with depolymerized MTs as a consequence of spindle checkpoint activation (Hoyt et al., 1991). The absence of MTs meant that the two SPBs of nocodazole-treated cells adopted a side-by-side configuration (Jacobs et al., 1988). Nocodazole washout triggered MT nucleation and subsequent MT polymerization. MT assembly did not change the intensity of the Tub4-yeGFP signal at SPBs in *TUB4-yeGFP mCherry-TUB1* cells (6/6 cells; Fig. 8 A) and *TUB4-yeGFP* cells (11/11 cells; Fig. 8 B). Similarly, neither did the signals from the γ-TuSC receptor Spc110 and the SPB core protein Spc42 change (12/13 and 9/11 cells; Fig. 8 B).

containing α-factor to remove nocodazole ($t = 0$). Images were acquired every 5 min to monitor MT renucleation. The enlargement on the bottom shows the detached cMT nucleation site with Spc72-yeGFP (green) and nucleated MTs (red). Images are single planes from z stacks. (D) Distribution of the numbers of tagged γ-TuSC proteins and Spc72 per single MT minus end plotted against the number of analyzed MTs. Mean number of molecules ± SEM, number of analyzed MTs (n), and number of independent datasets are given in the graphs. [Tub4]/[Spc97] and [Tub4]/[Spc98] indicate the ratio of Tub4 to Spc97 and Tub4 to Spc98, respectively. CI, confidence interval. Bars: (A, B, and C) 2 µm; (A and C, enlargements) 0.5 µm.

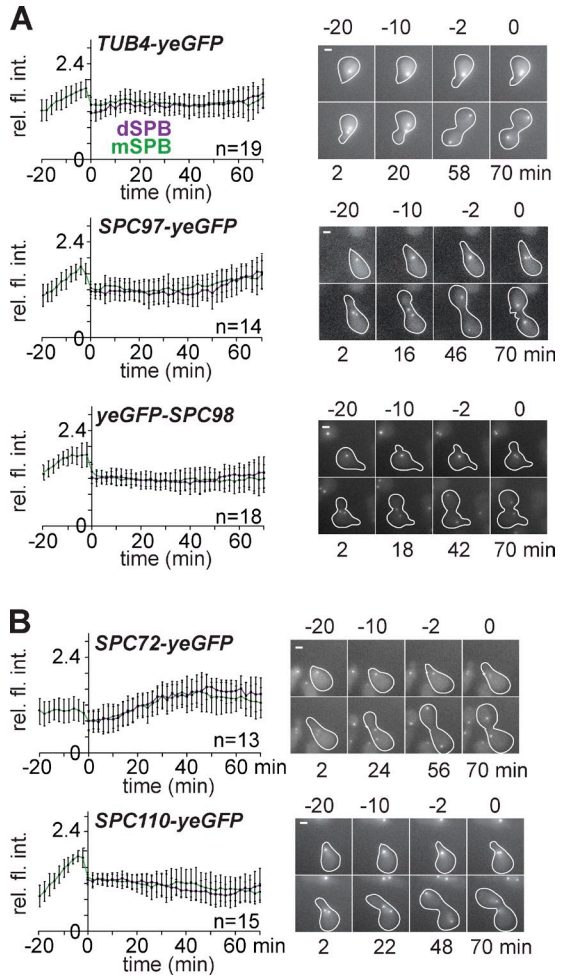

Figure 7. **Levels of γ-TuSC and receptors during the cell cycle.** (A, left) The signal intensity of the indicated yeGFP-tagged γ-TuSC proteins was analyzed by time-lapse analysis (graph of mean relative intensity with SD error bars) *n* is the number of cells, and *t* = 0 min indicates the time of SPB separation. The time of SPB duplication is indicated from *t* = −20 to *t* = 0 min. During this time interval, the measured signal is derived from two SPBs. dSPB, daughter SPB; mSPB, mother SPB. (right) Images from time-lapse videos of representative cells expressing the gene fusion indicated in the figure. (B) As in A but with *SPC72-yeGFP* or *SPC110-yeGFP*. (A and B) rel. fl. int., relative fluorescence intensity. Bars, 2 µm.

The concordance between these regrowth and cell cycle data (Fig. 7 A) indicates that the same number of γ-TuSC molecules are used for MT nucleation and MT anchorage.

Discussion

Relatively little is known about the stoichiometry and properties of MT nucleation sites in vivo. It is of particular interest whether a ring of 13 γ-tubulin molecules or a more extended γ-tubulin spiral nucleates MT and whether MT nucleation sites are homogenous and vary between cell cycle phases. Here, we used budding yeast as model system to address these issues. This system lends itself to this analysis because its MT nucleation and anchorage are entirely restricted to SPBs and it employs a minimal, but yet conserved, set of proteins: γ-tubulin, Spc97, Spc98, and the receptor proteins Spc110 and Spc72 (Geissler et al., 1996; Marschall et al., 1996; Spang et al., 1996; Knop et al., 1997; Chen et al., 1998; Knop and Schiebel, 1998; Nguyen et al., 1998). Our data show that at SPBs, the γ-TuSC assembles into a high-affinity stable platform of ∼17 γ-tubulin molecules that nucleates MTs. Based on these data, we suggest a modified template model (see following paragraphs).

Comparison of γ-tubulin behavior at centrosomes and SPBs

Measurements with rat kangaroo kidney (PtKG) cell lines expressing stable γ-tubulin–GFP showed a dramatic increase of centrosome-associated γ-tubulin as cells progressed through mitosis (Khodjakov and Rieder, 1999). This is not the case in budding yeast, where MT nucleation is probably restricted to G1/S phase of the cell cycle when the SPB duplicates (Marschall et al., 1996). Consistently, γ-tubulin levels at SPBs remained constant throughout the cell cycle. However, the recruitment of the γ-TuSC receptor Spc72 to SPBs was cell cycle regulated. This probably reflects the broader functions of Spc72 that include interactions with the checkpoint kinase Kin4 and the MT polymerase and XMAP215 homolog Stu2 (Chen et al., 1998; Usui et al., 2003; D'Aquino et al., 2005; Pereira and Schiebel, 2005; Caydasi and Pereira, 2009).

The dynamic properties of γ-tubulin–GFP in PtKG and yeast cells were similar. In PtKG cells, the FRAP signal of γ-tubulin–GFP recovered slowly in the 60 min after photobleaching and only recovered to 50–60% of the original signal (Khodjakov and Rieder, 1999). We observed a similar slow and partial recovery in budding yeast. In budding yeast, both the $t_{1/2}$ and Y_{max} values for γ-tubulin–GFP signals at SPBs were cell cycle dependent, suggesting that the SPB-associated γ-tubulin pool is subject to cell cycle–dependent regulation. Additional experiments that directly address the functional consequences of the phosphorylation of γ-TuSC components, Spc72, and Spc110 are required to understand this regulation (Keck et al., 2011; Lin et al., 2011).

The slow recovery of Tub4 in the FRAP experiments suggests a stable association of γ-TuSC with SPBs. This may indicate a slow recovery at SPBs even when γ-TuSCs are assembled into the minus ends of MTs. Alternatively, MTs are lost from the poles as a result of MT depolymerization, and, in response to this, γ-TuSCs are also lost. Renucleation of MTs would than lead to recruitment of new γ-TuSCs. The depolymerization model predicts that MT depolymerization increases γ-tubulin dynamics at SPBs or centrosomes. However, neither in PtKG cells nor in budding yeast was the recruitment of γ-tubulin–GFP to centrosomes affected by MT depolymerization (Khodjakov and Rieder, 1999). Moreover, removal of tubulin–γ-tubulin interactions by the *tub2-403* β-tubulin mutation in the presence of nocodazole only moderately affected the residency of γ-tubulin at SPBs, suggesting that γ-TuSC still stably binds to SPBs even in the absence of tubulin interactions. Finally, the observation that the dynamic properties of Tub4 at SPBs were similar in metaphase and anaphase cells although nMTs are clearly more dynamic in metaphase than in anaphase (Higuchi and Uhlmann, 2005) disfavors an important role of MT depolymerization for Tub4 dynamics at SPBs.

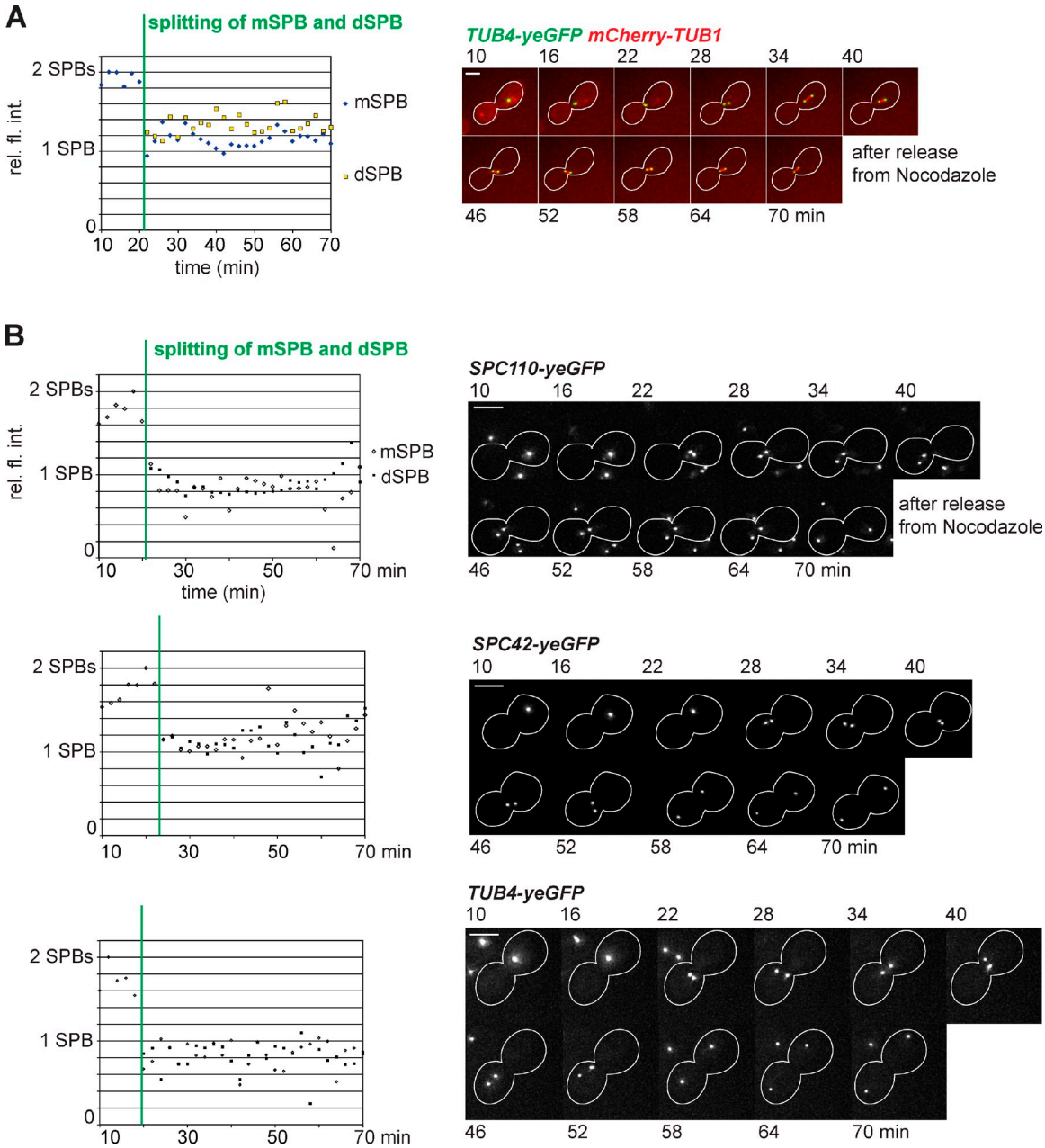

Figure 8. **Levels of γ-tubulin, nuclear receptors, and SPB core proteins during MT nucleation.** (A) MT renucleation assay of *TUB4-yeGFP mCherry-TUB1* cells. Nocodazole-arrested cells were released from the cell cycle block by washing the cells to remove nocodazole. The removal of nocodazole triggered MT renucleation. The relative fluorescence intensities (rel. fl. int.) of Tub4-yeGFP were quantified during the time of MT regrowth. The graph on the left shows relative intensities of Tub4-yeGFP at SPBs. Note that the Tub4-yeGFP SPB signal intensity is not changing during the experiment. Deconvolved images of the same cell are shown on the right. One representative experiment is shown. mSPB, mother SPB; dSPB, daughter SPB. (B) MT renucleation assay of *SPC110-yeGFP, Spc42-yeGFP, and TUB4-yeGFP* cells. Experiments were performed as in A. One representative experiment for each cell type is shown. Note that cells in B do not contain *mCherry-TUB1*. (A and B) Bars, 5 µm.

Analysis of the MT nucleation site in vivo

The template model was originally inspired by the ringlike appearance of the purified γ-TuRC from *Drosophila* (Zheng et al., 1995). According to this model, a ring of 13 γ-tubulin molecules functions as a direct template for the assembly of MTs with 13 tubulin protofilaments (Pereira and Schiebel, 1997; Kollman et al., 2011). In vitro studies using purified yeast γ-TuSC (Kollman et al., 2010) support the template model. In vitro, the γ-TuSC assembles into a spiral of 13 γ-tubulin molecules per turn when incubated with the N terminus of Spc110. The diameter and the helical pitch of the spiral are reminiscent of that of MTs. Furthermore, the plus ends of the γ-tubulin molecules in this spiral are fully exposed, enabling them to make longitudinal contacts with the α-tubulin subunit of the tubulin heterodimer.

Our in vivo assessments of the composition of MT nucleation sites on single detached MTs extend the template model. The in vitro data left the question of how extended the ring of γ-tubulin molecules is and whether the in vivo γ-tubulin template is composed entirely of γ-TuSC or contains additional

subunits, for example additional γ-tubulin molecules. This would be an attractive possibility, as γ-tubulin has the ability to interact with itself via lateral interactions (Aldaz et al., 2005). We measured 17 Tub4, 7 Spc97, and 9 Spc98 molecules on each nucleation site of single detached nucleation-competent cMTs. Similar Tub4 numbers were obtained using Cse4, Nuf2, or EGFP-VP2/VP6 as reference standards. The significance of the difference between the numbers of Spc97 and Spc98 and between the ratio of Tub4 and Spc97 on single MT minus ends was established by statistical tests. We excluded the possibility that the GFP moiety conferred folding problems upon the Tub4 fusion protein by comparing the signals of the very fast–folding *TUB4-sfGFP* with *TUB4-yeGFP*. A more than double excess of Tub4 over Spc97/Spc98 was also observed at SPBs.

Considering our measurements of single detached cMTs and the structural data on the γ-TuSC (Knop and Schiebel, 1997; Vinh et al., 2002), it is likely that seven γ-TuSCs, approximately three additional Tub4, and approximately two additional Spc98 molecules form the MT nucleation site in budding yeast. In addition, ∼15 Spc72 molecules were measured per MT nucleation site. Thus, a dimer of Spc72 interacts with one γ-TuSC. This raises the possibility that within an Spc72 dimer, one molecule interacts with Spc97 and the other with Spc98. This would be consistent with recorded two-hybrid interactions between Spc72-Spc97 and Spc72-Spc98 (Knop and Schiebel, 1998).

The Spc97/Spc98/Spc110 stoichiometry at SPBs is ∼1:1:2. This ratio suggests binding between one Spc110 dimer and one γ-TuSC molecule. However, because we do not know whether all of the Spc110 dimers at SPBs bind γ-TuSCs, other scenarios are possible. For example, an Spc110 dimer could link two γ-TuSC molecules by binding to Spc98 in each of two γ-TuSCs. This model is perhaps more consistent with the structural data on N-Spc110–induced γ-TuSC spirals (Kollman et al., 2010). In the latter case, the other half of the Spc110 molecules would not establish any contacts with the γ-TuSC. However, it is important to note that only an N-terminal fragment of Spc110 was used in the structural analysis. The full-length Spc110 embedded into the Spc42–Spc29 complex may behave differently (Elliott et al., 1999).

Our data give, for the first time, hints on how γ-tubulin and α/β-tubulin heterodimers interact at MT nucleation sites. We used the drug nocodazole to depolymerize MTs. Nocodazole binds to the same site in β-tubulin as colchicine (Ravelli et al., 2004). This high-affinity colchicine/nocodazole-binding site is absent from yeast γ-tubulin. The binding of the tubulin–nocodazole complex to SPBs requires the presence of γ-tubulin. This dependency indicates that the α/β-tubulin–nocodazole complex interacts with the γ-tubulin oligomer at SPBs. However, it is technically difficult to determine the number of α/β-tubulin heterodimers that remain associated with SPBs in cells incubated with nocodazole. Thus, we cannot be absolutely be sure that the FRAP measurements reflect the interaction between γ-tubulin and α/β-tubulin–nocodazole, as they could equally well reflect an interaction between tubulin and a stable γ-tubulin/tubulin assembly. However, the FLIP data do argue against this possibility, as the vast majority (>90%) of α/β-tubulin–nocodazole exchanges at SPBs. Thus, there is no indication for a stable γ-tubulin/α/β-tubulin–nocodazole ring at SPBs. In any case, in the presence of nocodazole, the interaction between α/β-tubulin heterodimers at SPBs exhibits a k_{off} = 0.094 s^{-1}, whereas the exchange at a growing MT plus end is in the range of k_{off} = 40 s^{-1} (Kosco et al., 2001; unpublished data). This is indicative of a more stable interaction between tubulin and γ-TuSC or γ-TuSC/α/β-tubulin at SPBs than the association between tubulin molecules at MT plus ends.

Finally, we establish that MT nucleation and MT attachment to the SPB, the two functions that are fulfilled by γ-tubulin complexes (Marschall et al., 1996; Kollman et al., 2010), require the same number of γ-tubulin molecules. Thus, the same γ-TuSC structure might support both processes without a need for structural rearrangements to invoke two states.

An extended model of the γ-tubulin nucleation site

A model for a nucleation site is illustrated in Fig. 9 A. Based on the convincing structural data presented by the Agard laboratory (Kollman et al., 2010), we suggest that a spiral of 13 γ-tubulin oligomers acts as a template for the formation of MTs. As outlined in the preceding paragraphs, we suggest that the nucleation site predominantly consists of seven γ-TuSC oligomers. This view is in agreement with the observation that γ-TuSCs can form oligomers in vitro (Kollman et al., 2010). However, our in vivo measurements indicate an excess of γ-tubulin and Spc98 over Spc97, suggesting that the nucleation site contains γ-tubulin and Spc98 molecules that are not assembled in the γ-TuSC. This surplus of γ-tubulin and Spc98 could be indicative of a specialized structure at the end of the γ-TuSC spiral that stabilizes the γ-TuSC ring or defines the position of the MT seam (Fig. 9 B). In this respect, it is important to note that budding yeast does not have the additional GCP4–6 molecules that have recently been proposed to execute specialized functions as end molecules in the mammalian γ-TuRC (Guillet et al., 2011; Kollman et al., 2011). It is tempting to speculate that the surplus of Spc98 in budding yeast takes over the role of GCP4 in the γ-TuRC of higher eukaryotes.

The γ-tubulin spiral determines the number of protofilaments per MT but also provides a high-affinity platform for tubulin assembly. Regulation of this platform will ultimately control MT nucleation. In this respect, it is interesting that γ-tubulin in the in vitro assembled γ-TuSC does not have a perfect fit for tubulin. Structural changes within the γ-TuSC, presumably in Spc98, will rotate the associated γ-tubulin such that it can perfectly interact with the α-tubulin subunit of tubulin (Kollman et al., 2010; Guillet et al., 2011). Recruitment of proteins to the γ-TuSC spiral or modifications of γ-TuSC components may induce such a conformational change. The detached cMTs of *kar1-Δ15* cells represent an excellent system to identify proteins that function together with the γ-TuSC in MT nucleation.

Materials and methods

Yeast methods

Standard protocols were used for genetic manipulations of *S. cerevisiae* cells (Guthrie and Fink, 1991). A PCR-based strategy was used for tagging yeast proteins at its endogenous locus with yeGFP (Janke et al., 2004).

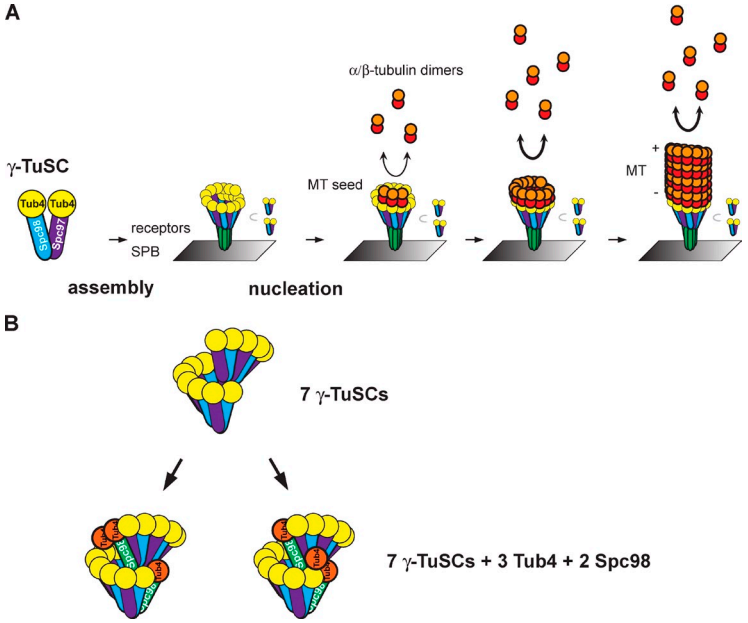

Figure 9. **Model for MT nucleation of γ-TuSCs at the SPB.** (A) An extended ring of 17 γ-tubulin molecules is assembled as a nucleation platform. This template is stably associated with the SPB in a cell cycle–dependent manner and further stabilized by the nucleation of MTs. Tubulin dimers interacting more strongly with γ-tubulin than with the MT plus end are the basis for MT nucleation. (B) Model of how the excess of Tub4 and Spc98 could stabilize the γ-TuSC ring.

mCherry-Tub1 and GFP-Tub1 encoded on yeast integration vectors were stably integrated into the yeast genome by homologous recombination (Straight et al., 1997; Khmelinskii et al., 2009). *pMet3* or *pGal1* promoter shut-off constructs of *CDC20* or *UPL-TEM1* were used to arrest cells in metaphase or anaphase, respectively (Mumberg et al., 1994; Shirayama et al., 1998; Shou et al., 1999). Overexpression of *SIC1* was used to arrest cells in G1/S (Schwob et al., 1994). All constructs and plasmids used to generate the yeast strains are listed in Table S1, and all yeast strains used in this study are described in Table S2. 0.01 mg/ml α-factor was used to arrest cell cycle progression in G1 or for synchronizing cell cycle progression of yeast cells. 0.01 mg/ml nocodazole was used for MT depolymerization of yeast cells. Expression from the *pGal1* promoter was switched off by transferring log-phase cells from a medium with 3% raffinose as a carbon source to a medium with 3% raffinose and 2% glucose. Transferring cells from synthetic deficient medium to synthetic complete (SC) medium with 2 mM methionine and cysteine repressed the *pMet3* promoter (Mumberg et al., 1994).

Growth curve and genetic interaction tests

Yeast cells were grown to log-phase in SC medium at 30°C unless otherwise stated. Budding indices were analyzed from ethanol-fixed cells with DAPI-stained DNA. Drop tests were prepared from cells grown for 1 d on YPAD plates or appropriate selection media at permissive temperatures. The strains were mixed with PBS adjusted to OD_{600} = 1, and 10-fold serial dilutions were spotted on appropriate agar plates that were incubated as indicated in the figure legend. Strains for analysis of genetic interactions were prepared by standard yeast genetics methods.

Microscopy and image analysis

Yeast strains used for live-cell imaging and photobleaching experiments were grown to log phase in sterile-filtered SC medium with an additional 100 mg/liter adenine sulfate at 30°C. Sterile-filtered YPAD was used in experiments to arrest cells with nocodazole. For imaging, cells were immobilized onto glass-bottom dishes. Dishes were incubated with 100 µl concanavalin A solution (6% concanavalin A, 100 mM Tris-Cl, pH 7.0, and 100 mM $MnCl_2$) for 5 min and subsequently washed with 300 µl of distilled water. Yeast cells were attached to the dish for 5–15 min at 30°C and subsequently washed and overlaid with prewarmed medium (SC or a 3:1 mixture of SC/YPAD for nocodazole-arrested cells). Fluorescent images were acquired with 2 × 2 binning on a DeltaVision RT system with softWoRx software (Applied Precision) equipped with a camera (Photometrics CoolSnap HQ; Roper Scientific), 100× UPlanSAPO objective with a 1.4 NA (Olympus), and a mercury arc light source. The 50-mW, 488-nm laser system (DeltaVision QLM; Applied Precision) was used for photobleaching experiments. All live-cell imaging and FRAP experiments were performed at 30°C. Data analysis was performed with the ImageJ software package (National Institutes of Health), and values obtained from measurements were further analyzed with Excel or GraphPad Prism software (GraphPad Software). For figure preparation, images were adjusted for brightness in Photoshop (Adobe) or ImageJ. If needed, deconvolution of the images was performed with the softWoRx software package (enhanced ratio algorithm with applied correction). Deconvolved microscopy images are shown in Figs. 2 B, 3 A, 5 (A–C), 8, and S3. Relative and absolute quantifications were performed from nonprocessed microscopy images, whereas analysis of localization of proteins was performed with deconvolved images.

Immunofluorescence of *tub2* mutants and *Δtub4* cells

Early log-phase cells grown in YPAD medium were synchronized with α-factor for 2 h and arrested in nocodazole for an additional 2 h. Tub4-degron auxin strains were further incubated in α-factor supplemented with 0.5 mM auxin for 30 min to induce degradation of Tub4–auxin-inducible degron (Nishimura et al., 2009), and all subsequent media contained 0.5 mM auxin. Approximately 5 × 10^7 cells were fixed with 3.5% formaldehyde in 100 mM KPO_4, pH 6.5, for 30 min at 37°C. Fixed cells were permeabilized by digestion of the cell walls with 16 U Zymolyase 20T (MP Biomedicals) in 100 mM KPO_4, 1.2 M sorbitol, 0.5 mM $MgCl_2$, and 71.5 mM β-mercaptoethanol until cells appeared dark by phase-contrast microscopy. Spheroblasts were immobilized on polylysine-coated (MP Biomedicals) multi-well slides and postfixed with methanol/acetone. After blocking with 1% BSA (Sigma-Aldrich) in PBS containing 100 mM lysine, cells were incubated overnight at 4°C in appropriately diluted mouse monoclonal antitubulin antibody (WA3) or rabbit anti-Tub4 antibody (a gift from J. Kilmartin, Medical Research Council Laboratory of Molecular Biology, Cambridge, UK) preparations. Primary antibodies were detected with anti–mouse Alexa Fluor 546–conjugated antibodies or anti–rabbit Alexa Fluor 647–conjugated antibodies. DNA was stained with DAPI. Fluorescent images were taken on the DeltaVision RT system as well and subsequently deconvolved, as described for live-cell imaging.

Time-lapse live-cell imaging

Cells were synchronized with α-factor for 1.5 cell cycles, attached to a glass-bottom dish, and released from the α-factor block by two washes with 2 ml of prewarmed SC medium. Image acquisition was started 10–15 min after release from the α-factor. Conditions for imaging were as follows: 15 stacks in the FITC channel, 0.1-s exposure, 0.3-µm stack distance, one reference image in brightfield channel with a 0.05-s exposure, and 61 frames in total every 2 min. Images were quantified by measuring the integrated density of the sum of projected videos for the region of interest (ROI) around the SPBs and a background region selected from outside the periphery of the analyzed cell. The mean intensity of the background was subtracted from the ROI. To correct for acquisition, bleaching signal intensities were divided by a bleaching factor. The bleaching factor was determined from the mean of three to five very short videos that had been generated with the same image acquisition conditions.

MT renucleation experiments were performed with α-factor–synchronized cells arrested with nocodazole for 1 h and 20 min. Nocodazole

was then washed out (t = 0), and cells were analyzed every 5 min for 30 min. Imaging conditions were as described above, with a 0.1-s exposure time in the red channel. 31 frames in total every 2 min were recorded, and images were analyzed by measuring integrated densities of maximum projected videos. Acquisition bleaching correction was performed as described above.

MT renucleation experiments of α-factor–arrested *kar1-Δ15* cells were performed with cells treated with nocodazole for 1 h. Subsequently, nocodazole was washed out with SC medium containing α-factor, and images were acquired every 5 min for 35 min to monitor MT renucleation. Imaging conditions described for preparation of linescans from single MTs were used. Images were deconvolved for the preparation of figures.

Measurements of beads and determination of point spread function (PSF)

For determination of the PSF TetraSpeck (Invitrogen), 100-nm beads were imaged under the following conditions: 21 stacks with 0.2-µm stack separation, a 0.1-s exposure in green channel with 10% transmission, and a 0.1-s exposure in red channel with 1% transmission. PSFs were determined from linescans of beads (plot profile function of ImageJ).

To assay the linearity of the microscope system, images were acquired under the following conditions: a 0.8-s exposure in the green channel with 10% transmission and 10 sections with 0.2-µm stack separation. Relative light intensities were calculated from maximum projection images from which electronic noise had been subtracted. Signal noise resulting from the electronic components of the microscope was calculated from the mean of 10 images recorded with the same shutter opening time but without illumination.

Specimen preparation for EM

kar1-Δ15 cells were processed as previously described (Höög and Antony, 2007), with minor modifications. In brief, *kar1-Δ15* cells were arrested with α-factor as described under Time-lapse live-cell imaging. After incubation, cells were collected onto a 0.45-µm polycarbonate filter (Millipore) using vacuum filtration and cryoimmobilised by high-pressure freezing using the EM PACT2 machine (Leica). The cells were then freeze substituted using the EM AFS2 device (Leica) with 0.1% glutaraldehyde, 0.2% uranyl acetate, and 1% water dissolved in anhydrous acetone and stepwise infiltrated with Lowicryl HM20 (Polysciences, Inc.). For polymerization, the samples were exposed to UV light for 48 h at −45°C and were gradually warmed to 20°C and left exposed to UV at room temperature for 48 h.

Electron tomography and modeling

Serial semithin sections (250 nm thick) were cut using a microtome (Reichert Ultracut S; Leica) and collected on Formvar-coated palladium-copper slot grids. 15 nm of gold-conjugated Protein A (Center for Molecular and Cellular Intervention University Medical Center Utrecht) was applied on both sides of the sections as tomographic-fiducial markers. Sections were then poststained with 2% uranyl acetate in 70% methanol and with lead citrate. Digital images were taken at 300 kV from a −60° to 60° tilt with a 1° increment on an electron microscope (Tecnai F30; FEI) equipped with an Eagle 4k charge-coupled device camera (pixel size of 1.499 nm at 15,500 magnification; FEI). Tomograms were then generated by R-weighted back projection, modeled, and analyzed using the IMOD software package (Kremer et al., 1996).

In vivo quantification of GFP-tagged proteins

GFP-tagged molecules were counted as previously described (Joglekar et al., 2006). To quantify GFP-tagged molecules at the SPB and KTs, cells with *CSE4-GFP* or *NUF2-GFP* and cells containing the gene of interest fused to GFP were mixed and adhered to glass-bottom dishes for imaging. The following conditions were used for imaging: 21 stacks, a 0.4-s exposure in the FITC channel, a 0.2-µm stack distance, and one reference image in the brightfield channel with a 0.05-s exposure. Only fluorescent clusters in the in-focus plane were used for the quantification (between stack 8 and 14). This was done to avoid errors as a result of declining fluorescence intensity with increasing distance of the objective to the coverslip. Relative fluorescent intensities were calculated from the mean intensities of a 5 × 5–pixel ROI in one image stack. The stack with the highest absolute signal intensity was used for measurement, and the brightest pixel was defined as the middle of the region used for quantification. A mean value of three areas of the same size as the ROI close to the cell was used for subtraction of the background. To calculate absolute numbers from the fluorescence intensity values, the relative values of the protein of interest were compared with values of *CSE4-GFP* or *NUF2-GFP* anaphase cells from the same dataset. To ensure that fluctuations in the mercury arc light source do not influence the measured values, datasets acquired on different days were compared.

To count GFP clusters at detached single MTs, *kar1-Δ15* cells with *mCherry-TUB1* and a yeGFP-tagged version of the protein of interest were treated with α-factor. Signals of anaphase *CSE4-yeGFP ste2Δ* cells pretreated as *kar1-Δ15* cells were used as a reference to calculate absolute protein numbers. The *kar1-Δ15* strain and *CSE4-yeGFP ste2Δ* cells were mixed and adhered to the same glass-bottom dish. The following conditions were used for imaging: 21 successive stacks of the FITC channel first and then the red channel with each 0.2-µm stack distance, a 1-s exposure in the FITC channel, a 0.9-s exposure in the red channel per stack, and one reference image in brightfield channel with a 0.05-s exposure. Only fluorescent clusters in the in-focus planes (between stack 8 and 14) were considered for quantification. This was done to avoid errors as a result of a decrease in fluorescence intensity with an increasing distance of the objective to the coverslip. Signals were measured from single-image planes.

A 5 × 5–pixel ROI with the maximum signal intensity in the center pixel was used to determine the mean relative fluorescence intensity, and a 7 × 7–pixel region surrounding the ROI was used for background subtraction. The mean signal intensities were calculated with the formula (as described in Johnston et al., 2010) $F_i = F_{ii} - (F_{io} - F_{ii}) \times (A_i/A_{io} - A_{ii})$, with F_{ii} and A_{ii} being the integrated fluorescence intensity of the inner square and the area of the inner square and F_{io} and A_{io} being the integrated fluorescence intensity of the outer square and the area of the outer square. To calculate absolute numbers from the fluorescence intensity values, the relative values of the protein of interest were compared with values of Cse4-yeGFP anaphase cells from the same dataset.

To measure Cse4-EGFP at KTs and Tub4-EGFP at the SPB and on single MTs with EGFP-VLP2/6 viral capsid proteins as a reference, the tagged viral particles and strains were mounted on different slides. Purified EGFP-VLP2/6 particles were provided by A. Charpilienne and D. Poncet (Virologie Moléculaire et Structurale, Unité Propre de Recherche du Centre National de la Recherche Scientifique, Gif-sur-Yvette, France; Charpilienne et al., 2001; Dundr et al., 2002). The viruslike particles were stored at 4°C at a concentration of 2 mg/ml in a solution of 20 mM Pipes and 10 mM Ca^{2+} + 0.5 M CsCl, pH 6.84. For mounting capsid proteins on slides, two tesa film strips (Beiersdorf) were transversally taped 0.5 cm apart on a slide, and a coverslip was gently pressed on top until the coverslip adhered. The virus capsid proteins were diluted 1:1,000 using 60 mM Pipes, 27.3 mM Hepes, and 10 mM $CaCl_2$, pH 7.0. The dilution was vortexed for 30 s, and 10 µl of the solution was perfused between the slide and coverslip. Both images of cells and virus particles were acquired on the same day within <2 h to avoid measurement errors as a result of fluctuations of the fluorescence light source of the microscope. The same imaging conditions used for calculation against Cse4-yeGFP as a reference were used for image acquisition (see above). Fluorescence intensities were calculated as described for a single MT (see above).

Linescan profiles of single MTs

Images were acquired as described for the quantification of a single MT. Here, however, the FITC and the red channel images were taken consecutively followed by the next stack. Images were deconvolved before analysis. MTs in single z stacks running parallel to the image plane were analyzed with ImageJ. Segmented lines were drawn along the MT, absolute light intensities were calculated with the plot profile command, and relative values for GFP and mCherry intensities were plotted in Excel (Microsoft).

FRAP experiments

The following protocol was used for FRAP experiments of arrested TUB4-yeGFP cells: five prebleach images, a 50-ms laser pulse with 100% laser power for bleaching, and images every 2 min over 60 min after bleaching and for G1/S phase cells every 1 min over 40 min after bleaching. Stack distance and exposure times were used as described under Time-lapse live-cell imaging.

For FRAP experiments of nocodazole-arrested *GFP-TUB1* cells, the following protocol was used: five prebleach images, a 50-ms laser pulse with 50% laser power for bleaching, and82 postbleach images with a 0.4-s exposure with a total experiment duration of 120 s. Before and after the experiment, one image was taken with a 0.5-s exposure in the red channel, a 0.4-s exposure in the green channel, and a 0.05-s exposure in brightfield to determine the localization of the SPB.

Fluorescence intensities of Tub4-yeGFP at the SPB were corrected with the Phair double normalization method (Phair et al., 2004). Normalized

intensities were fitted single to exponential curves ($y = y_0 + Ae^{-bx}$). Mobile fractions were calculated with the formula $Mob = -A/[1 - (y_0 + A)]$, and half recovery times were calculated using $-\ln 0.5/b$.

FLIP experiments

For FLIP experiments with *GFP-TUB1* strains, cells were arrested in nocodazole. Before bleaching, one image was acquired with a 0.6-s exposure in the red channel, a 0.05-s exposure in the brightfield channel, and a 0.4-s exposure in the green channel, and five prebleach images were collected with a 0.4-s exposure in the green channel. The daughter cell of a large-budded cell was continuously bleached with two 50-ms laser pulses with 100% laser power, and images were acquired before and after bleaching every 4 s with a 0.4-s exposure time in the green channel. Fluorescence intensities of a 5 × 5–pixel ROI around the SPB and of the whole cell were measured. A region outside the cell was used for background subtraction from ROI and the whole cell.

Online supplemental material

Fig. S1 shows growth tests and genetic interaction tests to show that GFP-tagged γ-TuSC proteins and receptors are functional. Fig. S2 shows further control quantifications of γ-TuSC proteins and receptors. Fig. S3 shows further examples of *kar1-Δ15* cells renucleating MTs in the cytoplasm. Fig. S4 shows electron tomographies of two additional α-factor–arrested *kar1-Δ15* cells. Tables S1 and S2 list plasmids (Table S1) and strains (Table S2) used in this study. Videos 1 and 2 (both related to Fig. S4) show a 3D model of the reconstructed *kar1-Δ15* cell (Video 1) and the tomogram of the cell (Video 2). Online supplemental material is available at http://www.jcb.org/cgi/content/full/jcb.201111123/DC1.

T. Stearns (Department of Biology, Stanford University, and Department of Genetics, Stanford School of Medicine, Stanford, CA) is acknowledged for providing *tub2-403* cells, E. Schwob (Institut de Génétique Moléculaire de Montpellier, Montpellier, France) for pGal1-*SIC1* constructs, and J. Kilmartin for anti-Tub4 antibodies. We are very grateful to A. Charpilienne and D. Poncet for providing purified EGFP-VP2/VP6 virus capsid proteins. We thank K. Bloom for communicating data before publication and T. Davis for discussion. We are thankful to S. Prugnaller from the European Molecular Biology Laboratory EM facility for helping us with image acquisition and modeling and H. Lorenz for advice on fluorescence microscopy. M. Knop (Zentrum für Molekulare Biologie der Universität Heidelberg, Heidelberg, Germany) is acknowledged for discussions and constructs and I. Hagan for reading the manuscript.

The work of E. Schiebel was supported by the grant from the Deutsche Forschungsgemeinschaft (Schi 295/4-1). S. Erlemann is a member of the Hartmut Hoffmann-Berling International Graduate School of Molecular and Cellular Biology.

Submitted: 25 November 2011
Accepted: 5 March 2012

References

Aldaz, H., L.M. Rice, T. Stearns, and D.A. Agard. 2005. Insights into microtubule nucleation from the crystal structure of human γ-tubulin. *Nature*. 435:523–527. http://dx.doi.org/10.1038/nature03586

Byers, B., K. Shriver, and L. Goetsch. 1978. The role of spindle pole bodies and modified microtubule ends in the initiation of microtubule assembly in *Saccharomyces cerevisiae*. *J. Cell Sci.* 30:331–352.

Caydasi, A.K., and G. Pereira. 2009. Spindle alignment regulates the dynamic association of checkpoint proteins with yeast spindle pole bodies. *Dev. Cell*. 16:146–156. http://dx.doi.org/10.1016/j.devcel.2008.10.013

Charpilienne, A., M. Nejmeddine, M. Berois, N. Parez, E. Neumann, E. Hewat, G. Trugnan, and J. Cohen. 2001. Individual rotavirus-like particles containing 120 molecules of fluorescent protein are visible in living cells. *J. Biol. Chem.* 276:29361–29367. http://dx.doi.org/10.1074/jbc.M101935200

Chen, X.P., H. Yin, and T.C. Huffaker. 1998. The yeast spindle pole body component Spc72p interacts with Stu2p and is required for proper microtubule assembly. *J. Cell Biol.* 141:1169–1179. http://dx.doi.org/10.1083/jcb.141.5.1169

Chenna, R., H. Sugawara, T. Koike, R. Lopez, T.J. Gibson, D.G. Higgins, and J.D. Thompson. 2003. Multiple sequence alignment with the Clustal series of programs. *Nucleic Acids Res.* 31:3497–3500. http://dx.doi.org/10.1093/nar/gkg500

Coffman, V.C., P. Wu, M.R. Parthun, and J.Q. Wu. 2011. CENP-A exceeds microtubule attachment sites in centromere clusters of both budding and fission yeast. *J. Cell Biol.* 195:563–572. http://dx.doi.org/10.1083/jcb.201106078

D'Aquino, K.E., F. Monje-Casas, J. Paulson, V. Reiser, G.M. Charles, L. Lai, K.M. Shokat, and A. Amon. 2005. The protein kinase Kin4 inhibits exit from mitosis in response to spindle position defects. *Mol. Cell*. 19:223–234. http://dx.doi.org/10.1016/j.molcel.2005.06.005

Dundr, M., J.G. McNally, J. Cohen, and T. Misteli. 2002. Quantitation of GFP-fusion proteins in single living cells. *J. Struct. Biol.* 140:92–99. http://dx.doi.org/10.1016/S1047-8477(02)00521-X

Elliott, S., M. Knop, G. Schlenstedt, and E. Schiebel. 1999. Spc29p is a component of the Spc110p subcomplex and is essential for spindle pole body duplication. *Proc. Natl. Acad. Sci. USA*. 96:6205–6210. http://dx.doi.org/10.1073/pnas.96.11.6205

Geissler, S., G. Pereira, A. Spang, M. Knop, S. Souès, J. Kilmartin, and E. Schiebel. 1996. The spindle pole body component Spc98p interacts with the γ-tubulin-like Tub4p of *Saccharomyces cerevisiae* at the sites of microtubule attachment. *EMBO J.* 15:3899–3911.

Giddings, T.H. Jr., E.T. O'Toole, M. Morphew, D.N. Mastronarde, J.R. McIntosh, and M. Winey. 2001. Using rapid freeze and freeze-substitution for the preparation of yeast cells for electron microscopy and three-dimensional analysis. *Methods Cell Biol.* 67:27–42. http://dx.doi.org/10.1016/S0091-679X(01)67003-1

Goodwin, S.S., and R.D. Vale. 2010. Patronin regulates the microtubule network by protecting microtubule minus ends. *Cell*. 143:263–274. http://dx.doi.org/10.1016/j.cell.2010.09.022

Guillet, V., M. Knibiehler, L. Gregory-Pauron, M.H. Remy, C. Chemin, B. Raynaud-Messina, C. Bon, J.M. Kollman, D.A. Agard, A. Merdes, and L. Mourey. 2011. Crystal structure of γ-tubulin complex protein GCP4 provides insight into microtubule nucleation. *Nat. Struct. Mol. Biol.* 18:915–919. http://dx.doi.org/10.1038/nsmb.2083

Guthrie, C., and G.R. Fink, editors. 1991. Methods in Enzymology: Guide to Yeast Genetics and Molecular Biology. Vol. 194. Elsevier Academic Press, San Diego, CA. 933 pp.

Higuchi, T., and F. Uhlmann. 2005. Stabilization of microtubule dynamics at anaphase onset promotes chromosome segregation. *Nature*. 433:171–176. http://dx.doi.org/10.1038/nature03240

Höög, J.L., and C. Antony. 2007. Whole-cell investigation of microtubule cytoskeleton architecture by electron tomography. *Methods Cell Biol.* 79:145–167. http://dx.doi.org/10.1016/S0091-679X(06)79006-9

Hoyt, M.A., L. Totis, and B.T. Roberts. 1991. *S. cerevisiae* genes required for cell cycle arrest in response to loss of microtubule function. *Cell*. 66:507–517. http://dx.doi.org/10.1016/0092-8674(81)90014-3

Hutchins, J.R., Y. Toyoda, B. Hegemann, I. Poser, J.K. Hériché, M.M. Sykora, M. Augsburg, O. Hudecz, B.A. Buschhorn, J. Bulkescher, et al. 2010. Systematic analysis of human protein complexes identifies chromosome segregation proteins. *Science*. 328:593–599. http://dx.doi.org/10.1126/science.1181348

Jacobs, C.W., A.E.M. Adams, P.J. Szaniszlo, and J.R. Pringle. 1988. Functions of microtubules in the *Saccharomyces cerevisiae* cell cycle. *J. Cell Biol.* 107:1409–1426. http://dx.doi.org/10.1083/jcb.107.4.1409

Janke, C., M.M. Magiera, N. Rathfelder, C. Taxis, S. Reber, H. Maekawa, A. Moreno-Borchart, G. Doenges, E. Schwob, E. Schiebel, and M. Knop. 2004. A versatile toolbox for PCR-based tagging of yeast genes: New fluorescent proteins, more markers and promoter substitution cassettes. *Yeast*. 21:947–962. http://dx.doi.org/10.1002/yea.1142

Jin, Q.-W., J. Fuchs, and J. Loidl. 2000. Centromere clustering is a major determinant of yeast interphase nuclear organization. *J. Cell Sci.* 113:1903–1912.

Joglekar, A.P., D.C. Bouck, J.N. Molk, K.S. Bloom, and E.D. Salmon. 2006. Molecular architecture of a kinetochore-microtubule attachment site. *Nat. Cell Biol.* 8:581–585. http://dx.doi.org/10.1038/ncb1414

Johnston, K., A. Joglekar, T. Hori, A. Suzuki, T. Fukagawa, and E.D. Salmon. 2010. Vertebrate kinetochore protein architecture: Protein copy number. *J. Cell Biol.* 189:937–943. http://dx.doi.org/10.1083/jcb.200912022

Keck, J.M., M.H. Jones, C.C. Wong, J. Binkley, D. Chen, S.L. Jaspersen, E.P. Holinger, T. Xu, M. Niepel, M.P. Rout, et al. 2011. A cell cycle phosphoproteome of the yeast centrosome. *Science*. 332:1557–1561. http://dx.doi.org/10.1126/science.1205193

Khmelinskii, A., J. Roostalu, H. Roque, C. Antony, and E. Schiebel. 2009. Phosphorylation-dependent protein interactions at the spindle midzone mediate cell cycle regulation of spindle elongation. *Dev. Cell*. 17:244–256. http://dx.doi.org/10.1016/j.devcel.2009.06.011

Khodjakov, A., and C.L. Rieder. 1999. The sudden recruitment of γ-tubulin to the centrosome at the onset of mitosis and its dynamic exchange throughout the cell cycle, do not require microtubules. *J. Cell Biol.* 146:585–596. http://dx.doi.org/10.1083/jcb.146.3.585

Kilmartin, J.V. 1981. Purification of yeast tubulin by self-assembly in vitro. *Biochemistry*. 20:3629–3633. http://dx.doi.org/10.1021/bi00515a050

Kitamura, E., K. Tanaka, S. Komoto, Y. Kitamura, C. Antony, and T.U. Tanaka. 2010. Kinetochores generate microtubules with distal plus ends: Their roles and limited lifetime in mitosis. *Dev. Cell*. 18:248–259. http://dx.doi.org/10.1016/j.devcel.2009.12.018

Knop, M., and E. Schiebel. 1997. Spc98p and Spc97p of the yeast γ-tubulin complex mediate binding to the spindle pole body via their interaction with Spc110p. *EMBO J.* 16:6985–6995. http://dx.doi.org/10.1093/emboj/16.23.6985

Knop, M., and E. Schiebel. 1998. Receptors determine the cellular localization of a γ-tubulin complex and thereby the site of microtubule formation. *EMBO J.* 17:3952–3967. http://dx.doi.org/10.1093/emboj/17.14.3952

Knop, M., G. Pereira, S. Geissler, K. Grein, and E. Schiebel. 1997. The spindle pole body component Spc97p interacts with the γ-tubulin of *Saccharomyces cerevisiae* and functions in microtubule organization and spindle pole body duplication. *EMBO J.* 16:1550–1564. http://dx.doi.org/10.1093/emboj/16.7.1550

Kollman, J.M., J.K. Polka, A. Zelter, T.N. Davis, and D.A. Agard. 2010. Microtubule nucleating gamma-TuSC assembles structures with 13-fold microtubule-like symmetry. *Nature*. 466:879–882. http://dx.doi.org/10.1038/nature09207

Kollman, J.M., A. Merdes, L. Mourey, and D.A. Agard. 2011. Microtubule nucleation by γ-tubulin complexes. *Nat. Rev. Mol. Cell Biol.* 12:709–721. http://dx.doi.org/10.1038/nrm3209

Kosco, K.A., C.G. Pearson, P.S. Maddox, P.J. Wang, I.R. Adams, E.D. Salmon, K. Bloom, and T.C. Huffaker. 2001. Control of microtubule dynamics by Stu2p is essential for spindle orientation and metaphase chromosome alignment in yeast. *Mol. Biol. Cell*. 12:2870–2880.

Kremer, J.R., D.N. Mastronarde, and J.R. McIntosh. 1996. Computer visualization of three-dimensional image data using IMOD. *J. Struct. Biol.* 116:71–76. http://dx.doi.org/10.1006/jsbi.1996.0013

Lawrimore, J., K.S. Bloom, and E.D. Salmon. 2011. Point centromeres contain more than a single centromere-specific Cse4 (CENP-A) nucleosome. *J. Cell Biol.* 195:573–582. http://dx.doi.org/10.1083/jcb.201106036

Lin, T.C., L. Gombos, A. Neuner, D. Sebastian, J.V. Olsen, A. Hrle, C. Benda, and E. Schiebel. 2011. Phosphorylation of the yeast γ-tubulin Tub4 regulates microtubule function. *PLoS ONE*. 6:e19700. http://dx.doi.org/10.1371/journal.pone.0019700

Marschall, L.G., R.L. Jeng, J. Mulholland, and T. Stearns. 1996. Analysis of Tub4p, a yeast γ-tubulin-like protein: Implications for microtubule-organizing center function. *J. Cell Biol.* 134:443–454. http://dx.doi.org/10.1083/jcb.134.2.443

Moritz, M., M.B. Braunfeld, V. Guénebaut, J. Heuser, and D.A. Agard. 2000. Structure of the gamma-tubulin ring complex: A template for microtubule nucleation. *Nat. Cell Biol.* 2:365–370. http://dx.doi.org/10.1038/35014058

Mumberg, D., R. Müller, and M. Funk. 1994. Regulatable promoters of *Saccharomyces cerevisiae*: Comparison of transcriptional activity and their use for heterologous expression. *Nucleic Acids Res.* 22:5767–5768. http://dx.doi.org/10.1093/nar/22.25.5767

Nguyen, T., D.B.N. Vinh, D.K. Crawford, and T.N. Davis. 1998. A genetic analysis of interactions with Spc110p reveals distinct functions of Spc97p and Spc98p, components of the yeast γ-tubulin complex. *Mol. Biol. Cell*. 9:2201–2216.

Nguyen, T.L., C. McGrath, A.R. Hermone, J.C. Burnett, D.W. Zaharevitz, B.W. Day, P. Wipf, E. Hamel, and R. Gussio. 2005. A common pharmacophore for a diverse set of colchicine site inhibitors using a structure-based approach. *J. Med. Chem.* 48:6107–6116. http://dx.doi.org/10.1021/jm050502t

Nishimura, K., T. Fukagawa, H. Takisawa, T. Kakimoto, and M. Kanemaki. 2009. An auxin-based degron system for the rapid depletion of proteins in nonplant cells. *Nat. Methods*. 6:917–922. http://dx.doi.org/10.1038/nmeth.1401

O'Toole, E.T., M. Winey, and J.R. McIntosh. 1999. High-voltage electron tomography of spindle pole bodies and early mitotic spindles in the yeast *Saccharomyces cerevisiae*. *Mol. Biol. Cell*. 10:2017–2031.

Pédelacq, J.D., S. Cabantous, T. Tran, T.C. Terwilliger, and G.S. Waldo. 2006. Engineering and characterization of a superfolder green fluorescent protein. *Nat. Biotechnol.* 24:79–88. (published erratum appears in *Nat Biotechnol.* 2006. 24:1170) http://dx.doi.org/10.1038/nbt1172

Pereira, G., and E. Schiebel. 1997. Centrosome-microtubule nucleation. *J. Cell Sci.* 110:295–300.

Pereira, G., and E. Schiebel. 2005. Kin4 kinase delays mitotic exit in response to spindle alignment defects. *Mol. Cell*. 19:209–221. http://dx.doi.org/10.1016/j.molcel.2005.05.030

Pereira, G., M. Knop, and E. Schiebel. 1998. Spc98p directs the yeast γ-tubulin complex into the nucleus and is subject to cell cycle-dependent phosphorylation on the nuclear side of the spindle pole body. *Mol. Biol. Cell*. 9:775–793.

Pereira, G., U. Grueneberg, M. Knop, and E. Schiebel. 1999. Interaction of the yeast γ-tubulin complex-binding protein Spc72p with Kar1p is essential for microtubule function during karyogamy. *EMBO J.* 18:4180–4195. http://dx.doi.org/10.1093/emboj/18.15.4180

Phair, R.D., S.A. Gorski, and T. Misteli. 2004. Measurement of dynamic protein binding to chromatin in vivo, using photobleaching microscopy. *Methods Enzymol.* 375:393–414. http://dx.doi.org/10.1016/S0076-6879(03)75025-3

Ravelli, R.B., B. Gigant, P.A. Curmi, I. Jourdain, S. Lachkar, A. Sobel, and M. Knossow. 2004. Insight into tubulin regulation from a complex with colchicine and a stathmin-like domain. *Nature*. 428:198–202. http://dx.doi.org/10.1038/nature02393

Schwob, E., T. Böhm, M.D. Mendenhall, and K. Nasmyth. 1994. The B-type cyclin kinase inhibitor p40SIC1 controls the G1 to S transition in *S. cerevisiae*. *Cell*. 79:233–244. http://dx.doi.org/10.1016/0092-8674(94)90193-7

Shirayama, M., W. Zachariae, R. Ciosk, and K. Nasmyth. 1998. The Polo-like kinase Cdc5p and the WD-repeat protein Cdc20p/fizzy are regulators and substrates of the anaphase promoting complex in *Saccharomyces cerevisiae*. *EMBO J.* 17:1336–1349. http://dx.doi.org/10.1093/emboj/17.5.1336

Shou, W., J.H. Seol, A. Shevchenko, C. Baskerville, D. Moazed, Z.W. Chen, J. Jang, A. Shevchenko, H. Charbonneau, and R.J. Deshaies. 1999. Exit from mitosis is triggered by Tem1-dependent release of the protein phosphatase Cdc14 from nucleolar RENT complex. *Cell*. 97:233–244. http://dx.doi.org/10.1016/S0092-8674(00)80733-3

Spang, A., S. Geissler, K. Grein, and E. Schiebel. 1996. γ-Tubulin-like Tub4p of *Saccharomyces cerevisiae* is associated with the spindle pole body substructures that organize microtubules and is required for mitotic spindle formation. *J. Cell Biol.* 134:429–441. http://dx.doi.org/10.1083/jcb.134.2.429

Straight, A.F., W.F. Marshall, J.W. Sedat, and A.W. Murray. 1997. Mitosis in living budding yeast: Anaphase A but no metaphase plate. *Science*. 277:574–578. http://dx.doi.org/10.1126/science.277.5325.574

Usui, T., H. Maekawa, G. Pereira, and E. Schiebel. 2003. The XMAP215 homologue Stu2 at yeast spindle pole bodies regulates microtubule dynamics and anchorage. *EMBO J.* 22:4779–4793. http://dx.doi.org/10.1093/emboj/cdg459

Vinh, D.B.N., J.W. Kern, W.O. Hancock, J. Howard, and T.N. Davis. 2002. Reconstitution and characterization of budding yeast γ-tubulin complex. *Mol. Biol. Cell*. 13:1144–1157. http://dx.doi.org/10.1091/mbc.02-01-0607

Wiese, C., and Y. Zheng. 2006. Microtubule nucleation: γ-Tubulin and beyond. *J. Cell Sci.* 119:4143–4153. http://dx.doi.org/10.1242/jcs.03226

Winey, M., C.L. Mamay, E.T. O'Toole, D.N. Mastronarde, T.H. Giddings Jr., K.L. McDonald, and J.R. McIntosh. 1995. Three-dimensional ultrastructural analysis of the *Saccharomyces cerevisiae* mitotic spindle. *J. Cell Biol.* 129:1601–1615. http://dx.doi.org/10.1083/jcb.129.6.1601

Wu, J.Q., and T.D. Pollard. 2005. Counting cytokinesis proteins globally and locally in fission yeast. *Science*. 310:310–314. http://dx.doi.org/10.1126/science.1113230

Zheng, Y., M.L. Wong, B. Alberts, and T. Mitchison. 1995. Nucleation of microtubule assembly by a γ-tubulin-containing ring complex. *Nature*. 378:578–583. http://dx.doi.org/10.1038/378578a0